2. DESIGN AND CONSTRUCTION OF THE PCCV MODEL

2.1 Design

The PCCV model design was directed by NUPEC with overall responsibility for the design and construction contracted to MHI, Tokyo. Responsibility for the design of the liner and penetrations was assigned to MHI's Kobe Shipyard and Machinery Works while the concrete portions of the model were subcontracted to Obayashi Corp., Tokyo.

The basic philosophy guiding the design of the PCCV model was agreed upon very early in the program [22]. Key elements of this design philosophy included:

1. The PCCV model would be a uniform 1:4-scale model of the prototype or actual prestressed concrete containment vessel of Ohi Unit 3.
2. Elements of the model that would affect the ultimate strength would be equivalent to the prototype. The model liner would be one-fourth the thickness of the prototype liner. Reinforcing ratios would be maintained and the number and arrangement of the prestressing tendons would, to the extent possible, be identical to the prototype.
3. The model would be capable of reproducing the failure modes postulated for the prototype, including
    a. Hoop tensile failure of the cylinder wall
    b. Bending-shear failure at the junction of the cylinder wall with the basemat
    c. Shear failure in the basemat above the tendon gallery
    d. Bearing failure at the tendon anchors
    e. Bending-shear failure at the large penetrations
    f. Bending-shear at the small penetrations
    g. Liner tearing due to strain concentrations at local discontinuities (stiffeners/anchors, thickened reinforcing plates at penetrations and embedments)
    h. Leakage at penetration seals due to ovalization or distortion of the sealing surfaces.

Furthermore, to the extent possible, introduction of non-representative failure modes as a result of scaling or other modeling artifacts was to be avoided.

The general arrangement and representative failure mode locations are shown in Figure 2.1.

While the PCCV model was not 'designed' in the conventional sense, it's features were scaled directly from the Ohi-3 design with some simplifications to facilitate construction without compromising the objectives of the test. The prototype, Ohi-3, was designed in accordance with the "Draft Technical Code for Concrete Containment Vessels in Nuclear Power Plants" issued by Ministry of International Trade and Industry/Agency for Natural Resources and Energy (MITI/ANRE) in November, 1981 [23]. This draft code was formally adopted in 1993 as MITI Notification No. 452. The code is not identical to the American Society of Mechanical Engineers/American Concrete Institute (ASME/ACI) code [9], which governs the design of concrete containments in the U.S.; however, the basic design philosophies are similar, i.e., to ensure that all elements of the containment structure respond elastically (with some minor exceptions for secondary stresses) to the specified design loading conditions.

Construction of the prototype was also governed by Japanese Architectural Standard Specifications No. 5 and 5N for Reinforced Concrete Work at Nuclear Power Plants [24, 25]. Construction specifications for the PCCV model also followed these standards to the extent possible; however, modifications were made to adapt the specifications to U.S. construction practices.

The final design drawings for the PCCV model are provided in Appendix A. While it is beyond the scope of this report to include all the details of the design and construction specifications, a discussion of those features relevant to the model's response is appropriate and is included below.

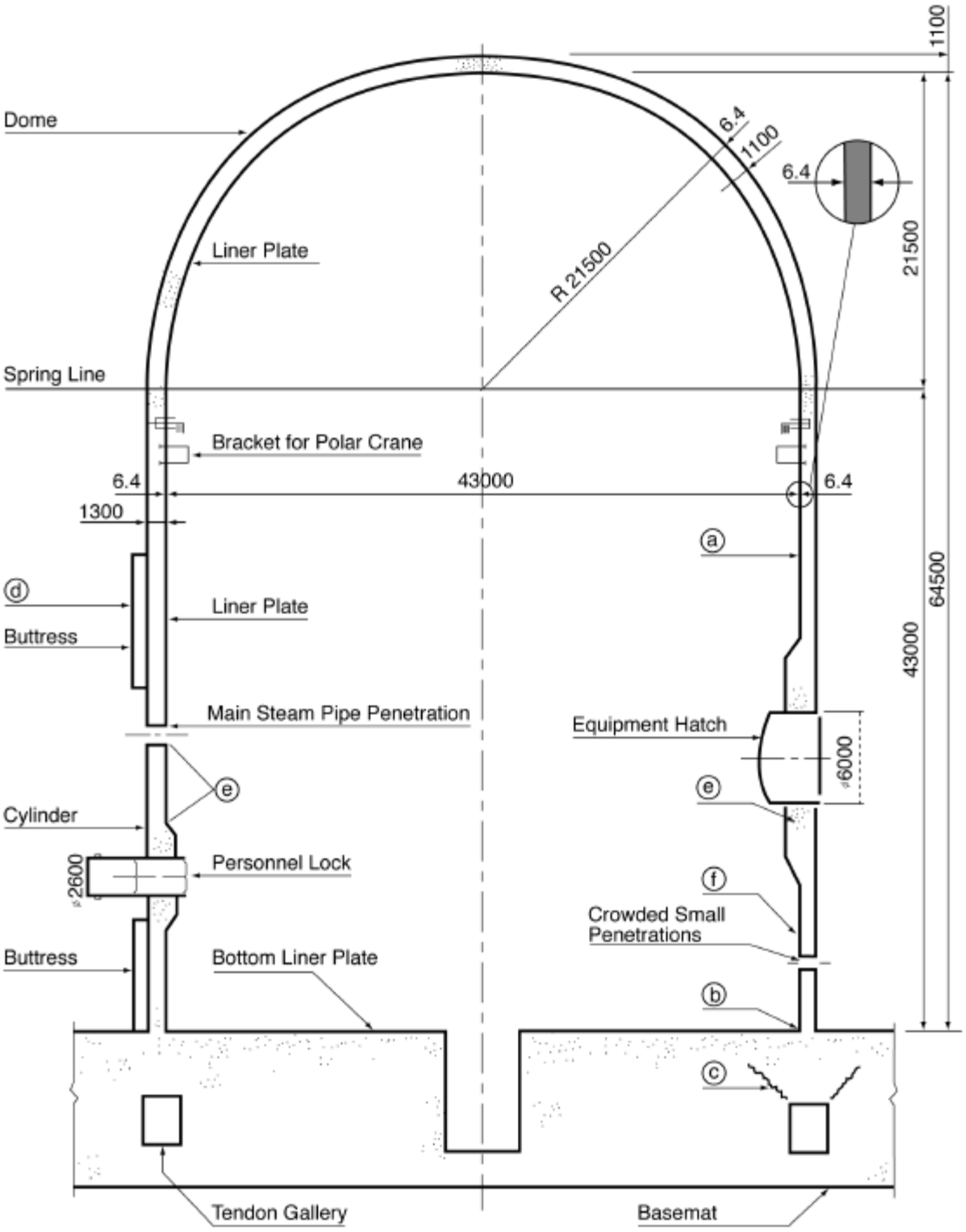

Figure 2.1. Elevation of PCCV Prototype and Potential Failure Locations

2.1.1 Liner Design Considerations

Design and fabrication/erection of the liner and penetrations was performed by MHI. The detailed specifications and practices are included in the project files. Essentially, the 1.6 mm (1/16") model liner was scaled from the 6.4 mm (~1/4") prototype liner. The as-built model liner thickness was 1.8 mm (0.070"), the extra 0.2 mm (0.008") providing a fabrication allowance. The model and prototype liner were both fabricated from SGV 410[1] carbon steel. JIS G3118 does not specify plate material under 6mm in thickness. The PCCV liner plate was fabricated to the same specifications as SGV410. Liner anchors and stiffeners were fabricated from SS 400[2]. Penetration assemblies were fabricated from SGV 410. The nominal properties of SGV 410 and SS 400 are given in Table 2.1. Miscellaneous non-structural components, e.g. back-up bars, were fabricated from U.S. common bar stock, typically ASTM A36 carbon steel.

Table 2.1 Properties of Liner Materials

Nominal Properties	Liner Plate	Liner Anchors
	SGV 410	SS 400
Yield Strength	225 Mpa (33 ksi)	235 Mpa (34 ksi)
Tensile Strength	410 MPa (59 ksi)	392 Mpa (57 ksi)

The liner material was procured in Japan, and liner panels were prefabricated and welded at MHI's Kobe Shipyard. Jigs, to support the liner panels and facilitate field erection and assembly, were attached to the liner panels prior to shipping them to the test site in Albuquerque, NM. Note that these jigs are unique to the construction of the model. The prototype liner is thick enough to be self-supporting without the use of any jigs. All vertical and horizontal liner weld seams in the prototype were reproduced in the model. Typically, the panel assemblies for the cylinder wall fabricated in Kobe encompassed three vertical rings of individual plate segments, resulting in assemblies approximately 3 m^2. Dome segments and penetration assemblies were typically smaller, individual plate segments. All welding of the assemblies in Kobe, including attachment of the anchors and stiffeners, was done by computer-controlled automatic welders. All shop welding was done without the use of back-up bars.

Standard coupons were made from the liner and liner anchor materials, and these specimens were tested for quality control purposes and to determine the actual material properties. The results of these tests are summarized in Appendix B.

The general arrangement of the liner anchors on the PCCV model is shown in the design drawings and is illustrated in Figure 2.2. The vertical liner anchors in the prototype consisted of 'T-anchors' spaced 600 mm (24") on-center throughout the cylinder wall and dome. These anchors are built-up sections, continuously welded to the liner plate with double-sided fillet welds. Horizontal bar stiffeners are provided above and below each horizontal weld seam to stiffen the liner during construction. The model liner anchors and stiffeners are 1:4-scale of the prototype. At 1:4-scale, the vertical anchor spacing would be 150 mm (6"); however, because the liner anchors are, in general, ineffective at resisting pressure and facilitating fabrication, the vertical anchor spacing was increased to 450 mm (18") except near discontinuities in the liner, such as the wall-base junction, around the E/H, A/L, M/S, and F/W penetrations and around the crane rail bracket embedments, as shown in Figure 2.2. Furthermore, the vertical liner anchors were not extended into the dome. T-stiffeners were used at the perimeter of the dome liner segments, but interior T-anchors were replaced with small stud-type anchors, as shown on the drawings. Again, since the strains in the dome were expected to be well below those experienced by the cylinder wall, this modification was not judged to affect the pressure capacity of the model.

As noted previously, the majority of the liner anchors were shop-welded to the liner using welding machines. One additional deviation from the prototype was the use of intermittent, staggered fillet welds to attach the anchors and stiffeners to the liner plate. There was a concern that these 'stitch' welds might generate additional local strain concentrations from the weld geometry itself. Therefore, anchors and stiffeners adjacent to other local liner discontinuities were continuously welded to reduce the possibility of premature liner tearing.

---

[1] Japanese Industrial Standard (JIS) G 3118, "Carbon Steel Plates for Pressure Vessels for Intermediate and Moderate Temperature Service," Japanese Standards Association.
[2] JIS G 3101, "Rolled Steel for General Structure," Japanese Standards Association.

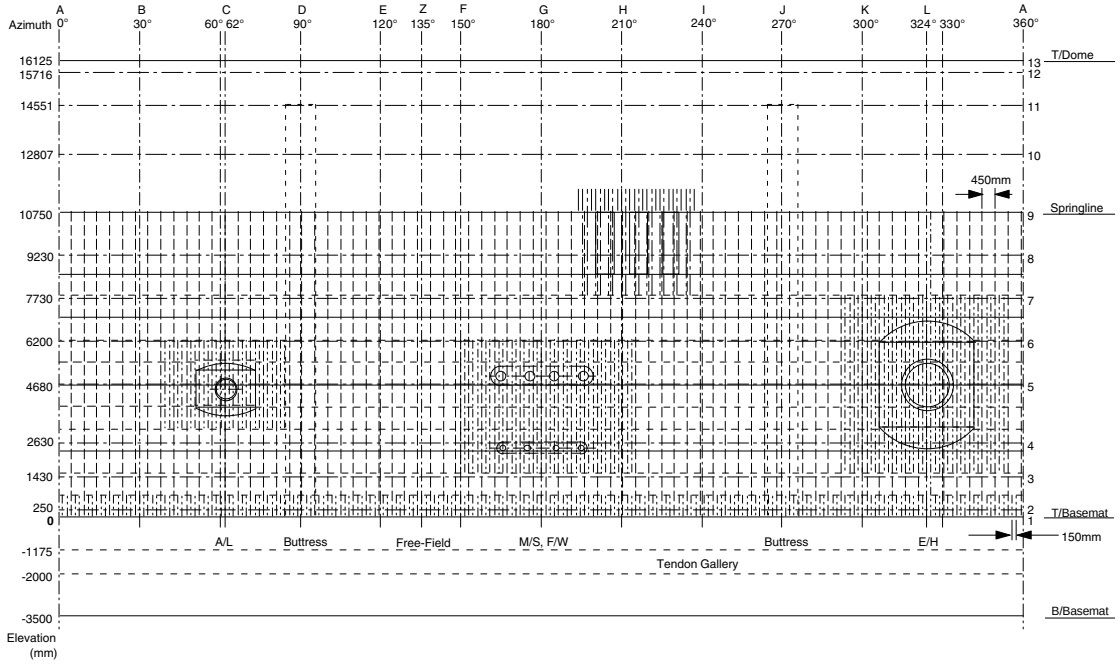

Figure 2.2 Liner Anchor Layout

While all the penetrations in the prototype were not included in the model, the major penetrations, consisting of the E/H, A/L, M/S, and F/W penetrations, were included in the model. These penetrations were representative of all the penetrations in the prototype and would be capable of reproducing the local strain concentrations in the structure and the liner. The E/H and A/L penetration assemblies in the model are 1:4-scale functional representations of the prototype assemblies, except that the A/L assembly includes only a single pressure seating cover and the interior doors are not reproduced. The model M/S and F/W penetration assemblies only included the penetration sleeve and reinforcing plates and were equipped with an interior flange and sealed with bolted pressure seating blind cover. No attempt was made to simulate the constraint conditions that might be imposed by the M/S or F/W piping. All the penetration sealing surfaces were milled and machined with groves for double O-ring gaskets. The prototype penetration assemblies are shown in Figures 2.3 to 2.6 for comparison to the model penetration assemblies shown in the design drawings. The model did not include the polar crane rail or brackets; however, a set of three adjacent bracket embedments were included to reproduce the local discontinuities in the liner.

The erection, field welding, and quality control of the liner are described in Section 2.2.

2.1.2 Concrete Design Considerations

2.1.2.1 Geometry

While the basic geometric scale of 1:4 was maintained throughout the PCCV model, some exceptions and modifications were required. Most significantly, the configuration of the model basemat had to be determined. The thickness of the model basemat at 1:4 scale is 3.5 m (11' 5-3/4"). The primary design consideration of the model basemat is that the rotational stiffness at the wall-base junction is equivalent to the prototype, since this affects the bending-shear failure mode at this location. The prototype containment basemat is continuous with the mat for the surrounding structures and includes a large reactor cavity at the center of the containment. Simplified three-dimensional finite element analyses of both the prototype and model subjected to pressure loading were performed to select the dimensions and reinforcement for the model basemat that would yield the desired response characteristics. The scaled basemat thickness of 3.5 m was maintained and, with the reactor cavity eliminated from the model, the radius of 7.2 m (23' 7 ½")and reinforcing were selected to match rotational stiffness of the prototype.

The location and size of the tendon gallery were scaled from the prototype. However, some modification of the construction sequence was required to accommodate this decision. Since the vertical prestressing tendons could not be inserted and tensioned inside a roughly 1-m^2 (2'-1" × 2'-8") tunnel, the portion of the basemat outside and below the tendon gallery was not constructed until after the tendons had been tensioned. This resulted in a somewhat different state of stress in the model basemat after prestressing; however, this difference was not significant and was unavoidable. Four access 'tunnels' to the tendon gallery were also included at 0 degrees, 90 degrees, 180 degrees, and 270 degrees to allow for visual inspection of the vertical tendon anchors and to ventilate the tendon gallery to minimize moisture that might affect the tendon anchors and the instrumentation.

Finally, some minor modifications in the geometry of the hoop tendon buttresses were required to accommodate the prestressing hardware. These were again judged to be insignificant with respect to the model's response to pressure.

2.1.2.2 Concrete Mix

The fundamental requirement of the PCCV model concrete was that it exhibit the same properties as the concrete used in the prototype. Based on prior experience with the construction and testing of a 1:6-scale reinforced concrete containment model at SNL, the approach to achieving this requirement was to specify a mix, using local (New Mexico) materials that would have the same 91-day[3] compressive strength (f_c') as the prototype concrete and then test the trial mix(es) to ensure they exhibited the same mechanical and chemical properties.

Two different concrete strengths were used in the prototype: 300 kg/cm^2 (4300 psi) for the majority of the basemat and 450 kg/cm^2 (6400 psi) for the cylinder wall, dome, and the portion of the basemat above the tendon gallery. The location of each mix, along with the lifts used in the construction of the model, are shown in Figure 2.7. Note that concrete lifts were not scaled from the prototype and are unique to the model.

The mix designs for the PCCV model consisted of Type I-II cement, air-entrained with 20% Class 2 Flyash and superplasticizer. Cement, aggregate, flyash, and water were all obtained locally and were batched by a supplier and mixed in transit. Maximum aggregate size was 10 mm (3/8"). Water/cement ratio for the 300 and 450 kgf/cm^2 mixes were 0.43% and 0.34%, respectively.

Corrosion due to the presence of chlorides and alkalis in the mix was a concern for the prototype due to the close proximity of the plant to the ocean; however, this was not judged to be a major concern for the model, although the chemical composition of the mix would be tested. Flyash was specified for the trial mix, since the use of flyash is standard practice in the construction of Japanese nuclear power plants and minimizes possible reaction and expansion of the aggregate. (Use of flyash is not permitted in construction of U.S. nuclear power plants). Superplasticizers were specified to facilitate placement of the concrete by pumping in congested areas. A maximum slump of 10 cm (4") before and 20 cm (8") after adding superplasticizers at the site was specified.

The trial mixes were batched and tested by Construction Technologies Laboratories, Skokie, IL to determine if they met the project specifications. The properties determined from trial mix specimens are summarized in Appendix B. In lieu of actual material property data, the trial mix properties were used for the pretest analysis of the PCCV model.

Quality control and material property test results for the concrete used to construct the model are described in Section 2.2 and summarized in Appendix B.

2.1.2.3 Reinforcing Steel (Rebar)

Normal, i.e. non-tensioned reinforcing steel for the prototype included grade SD490, SD390, and SD345 deformed bars[4]. The same grade steels were used to manufacture the rebar for the model in the U.S. (Cascade Steel, McMinnville, OR) in accordance with JIS Standards. The nominal properties for the rebar used in the model are summarized in Tables 2.2 and 2.3.

---

[3] JIS A 1108, "Method of Test for Compressive Strength of Concrete," allows specification of design strength at four weeks (28 days) or 13 weeks (91 days). Project specifications for the PCCV prototype and model specified the design strength f_c' at 91 days.

[4] JIS G 3112, "Steel Bars for Concrete Reinforcement."

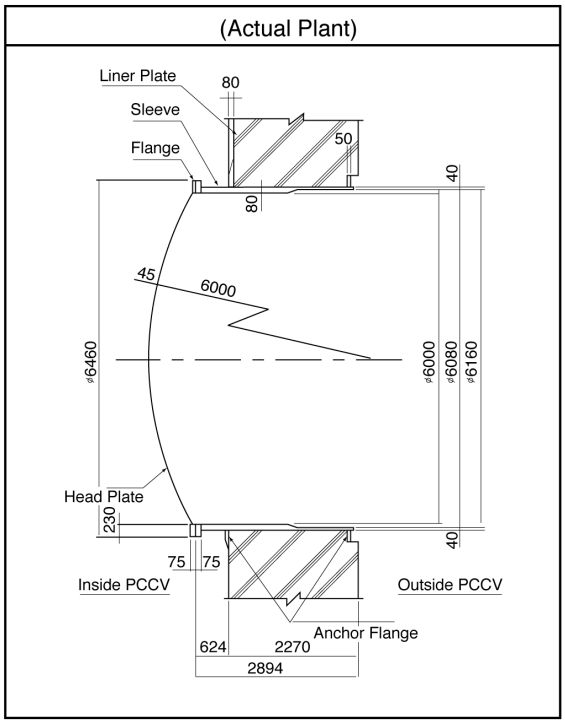

Figure 2.3 PCCV Prototype Equipment Hatch Arrangement

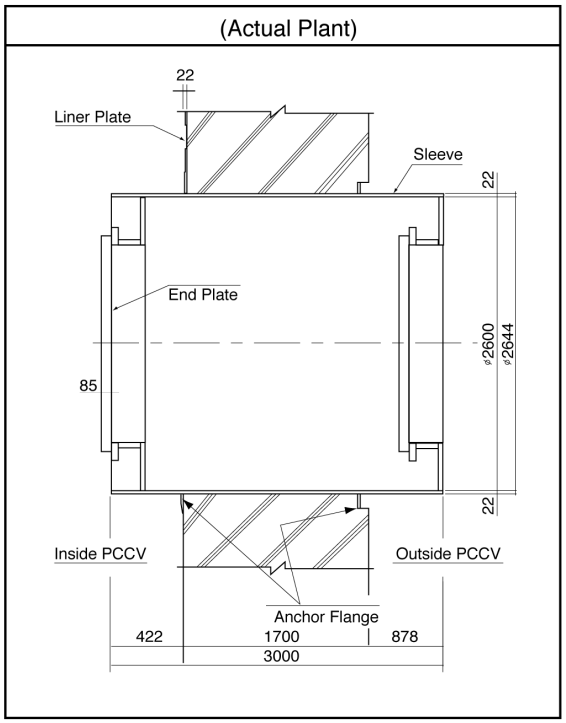

Figure 2.4 PCCV Prototype Personnel Airlock Arrangement

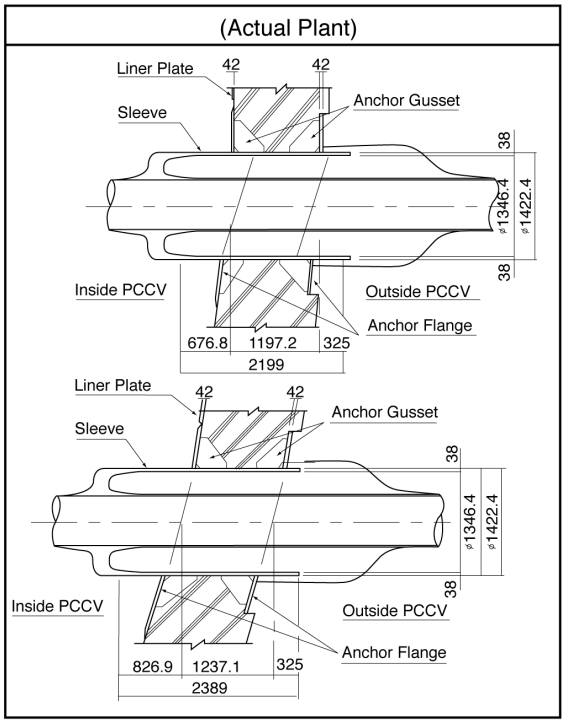

Figure 2.5 PCCV Prototype Main Steam Penetration Arrangement

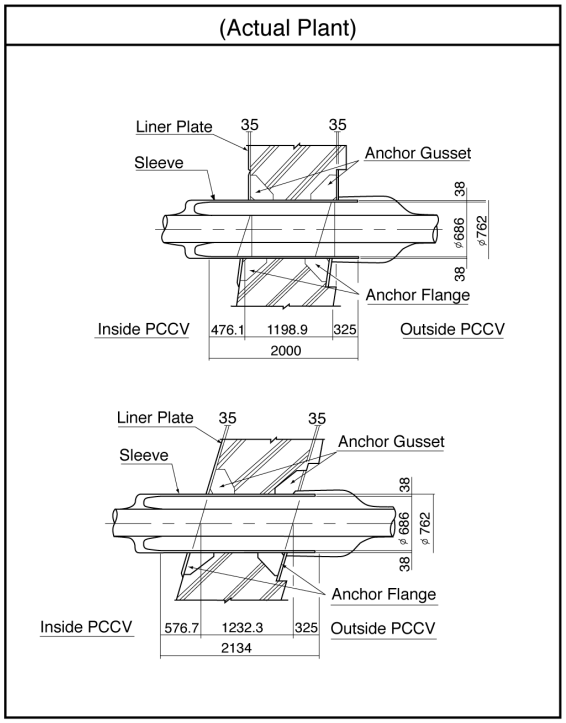

Figure 2.6 PCCV Prototype Feed Water Penetration Arrangement

In order to minimize rebar congestion in the model, all splices were originally intended to be made using swaged threaded couplers or position threaded couplers[5]. Swaged in-place couplers were not considered practical for the model due to limited clearance for the hand press. However, field considerations required some limited use of this type of coupler[6].

Samples of all the rebar used in the model were tested for quality control and to determine mechanical properties for analysis according to JIS and ASTM methods. Tests were also conducted of both the threaded and position-threaded couplers used in the model construction. (No tests were conducted of the swaged in-place couplers.) 'Dumbbell' specimens were machined from SD390 D16, and D22 bars to measure the basic material properties. Finally, a series of bars were tested with strain gages installed in the same manner as the instrumented bars in the model to calibrate the strains with a standard extensometer. The results of all these tests are summarized in Appendix B.

While the basic reinforcing ratios in the model were nearly the same as the prototype, the reinforcing in the model differed from the prototype. Individual bars in the model were not scaled directly from the prototype. Generally, in the containment shell (i.e. the cylinder wall and dome), the rebar was placed in one layer in each direction on each face. Figure 2.8 compares the arrangement of the reinforcing at the base of the cylinder wall in the prototype with the model. In-plane spacing of the rebar in the model is based on the arrangement of the prestressing tendons (2 degrees on center circumferentially and 112.5 mm (4.4") on center vertically). Bar sizes were then selected to reproduce as closely as possible, within the limits of the standard bar sizes available, the reinforcing ratio of the prototype.

Tolerances on formed surfaces and placement of rebar were developed by considering the 1:4-scaled tolerances for the prototype and then adjusting these to accommodate practical construction limitations, such as congestion and clearance for concrete placement. These tolerances are specified in the model construction specifications along with the as-built records. The deviations from the nominal design dimensions were not judged significant enough to affect the response of the model and, accordingly, are not included in this report.

Additional reinforcing was also provided around the penetrations in the model. However, where prototype penetrations were eliminated, no additional reinforcing was included in the model.

2.1.3 Prestressing Design Considerations

Since the unique feature of the PCCV model, compared to previous large-scale containment model tests, was the prestressing system, particular attention was paid to the design, construction, and instrumentation of this component. An unbonded, seven-wire strand prestressing system[7] was used in both the PCCV prototype and model. The tendons in the prototype consisted of 55, 12.7mm (½ in) diameter seven-wire strands[8]. The number and arrangement of the tendons in the model were kept the same as the prototype. The arrangement of the tendons is shown in Appendix A.

Both the prototype and model tendons were inserted in galvanized metal sheath or ducts after the concrete had been placed and allowed to cure, then tensioned. The model ducts were, generally, 35 mm (1-3/8") in diameter and were not 'greased' after tensioning. (The prototype tendon ducts were, as typical of most unbonded tendons, injected with a heavy grease after tensioning to protect the tendons from corrosion. Since the model tendons would only be in use for a relatively short time (< 2 years), they were not greased, although an anti-corrosion 'shop-coat' was brushed on prior to insertion in the ducts. Not greasing the tendons also facilitated the placement of instrumentation on selected tendons.)

In order to maintain the correct scaled cross-sectional area, the model tendons consisted of three, 13.7-mm (0.54") seven-wire strands. These model strands were custom-manufactured by the vendor for the model and nominal properties are not defined in the Japanese standard specifications, although the basic wire material was the same used for the prototype tendons[9]. The minimum properties of the model strands per the project specifications are given in Table 2.4. Extensive testing of individual strands as well as the tendon system were conducted for quality control and to determine the mechanical properties of the tendons. The results of these tests are summarized in Appendix B.

---

[5] Grip-Twist®System, manufactured by BarSplice Products Co., Dayton OH.
[6] Bar-Grip®System, ibid
[7] VSL Multistrand Posttensioning Systemâ, VSL Corporation, Japan
[8] JIS G 3536, "Uncoated Stress-Relieved Steel Wires and Strands for Prestressed Concrete."
[9] JIS G 3502, "Piano Wire Rod."

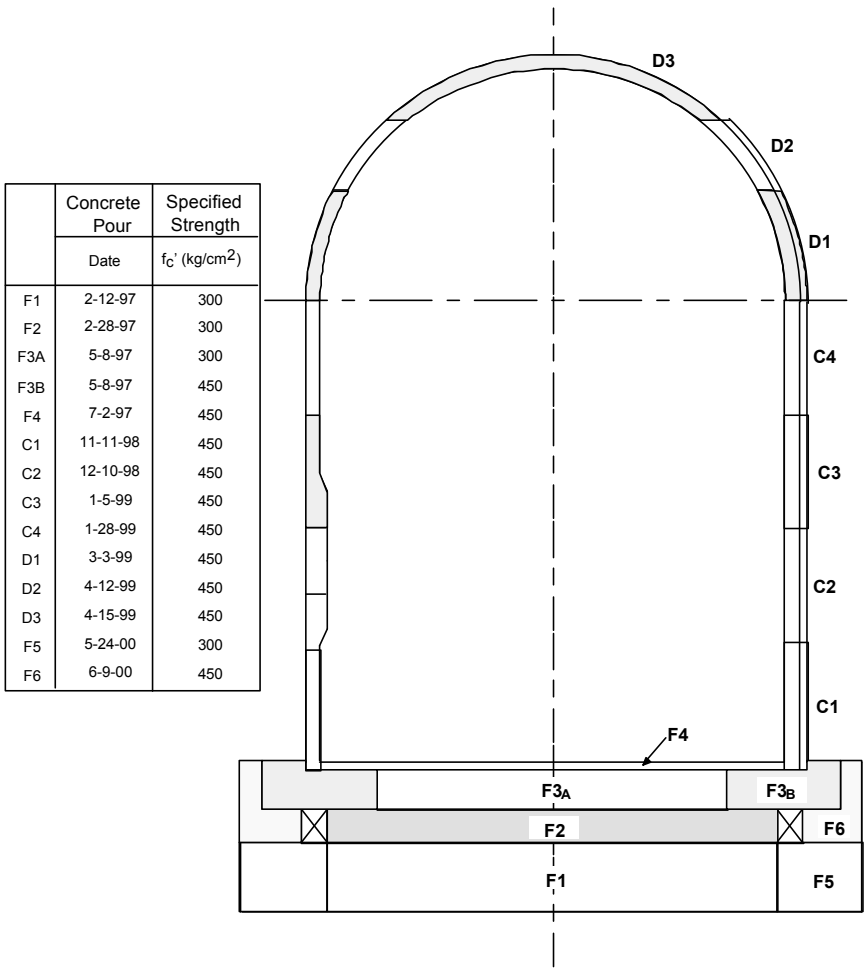

	Concrete Pour	Specified Strength
	Date	f_c' (kg/cm^2)
F1	2-12-97	300
F2	2-28-97	300
F3A	5-8-97	300
F3B	5-8-97	450
F4	7-2-97	450
C1	11-11-98	450
C2	12-10-98	450
C3	1-5-99	450
C4	1-28-99	450
D1	3-3-99	450
D2	4-12-99	450
D3	4-15-99	450
F5	5-24-00	300
F6	6-9-00	450

Figure 2.7 PCCV Concrete Lifts and Strengths

Table 2.2 JIS G 3112 Reinforcing Steel Properties

Grade	SD345	SD390	SD490
Model Location	Shell shear ties	Shell main bars, basemat shear bars	Basemat main bars
F_y min	343MPa ~50 ksi	392MPa ~57 ksi	490MPa ~71 ksi
F_t min	490MPa ~71 ksi	559MPa ~81 ksi	618MPa ~90 ksi
Elong.	18-20%	16-18%	12-14%

Table 2.3 JIS G 3112 Bar Properties
(Comparison with ASTM Standard Rebar)

	Nom. Diameter (d)		Nom. Area		Nom. Weight	
	millimeters	in	cm^2	in^2	kg/m	lb/ft
D6 (#2)	6.35	0.25	0.317	0.05	0.25	0.17
D10 (#3)	9.53	0.375	0.713	0.11	0.56	0.38
D13 (#4)	12.7	0.5	1.267	0.2	1	0.67
D16 (#5)	15.9	0.626	1.986	0.31	1.56	1.05
D19 (#6)	19.1	0.752	2.865	0.44	2.25	1.51
D22 (#7)	22.2	0.874	3.871	0.6	3.04	2.04

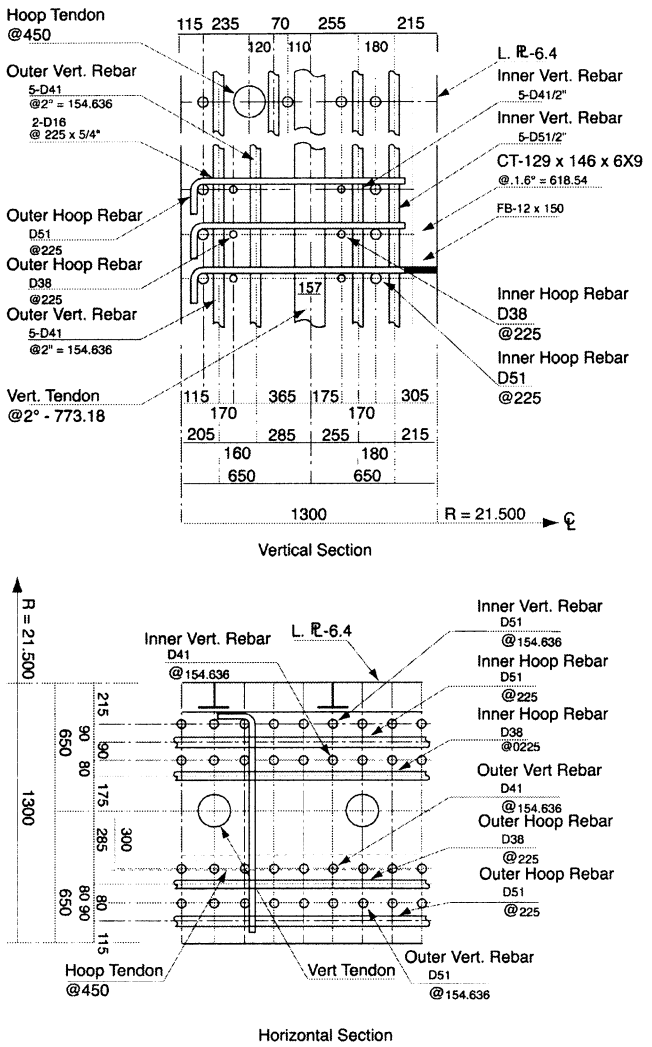

Figure 2.8 Arrangement of Reinforcing in the PCCV Prototype and Model at the Wall-Base Junction

Table 2.4 PCCV Model Tendon Strand Properties

Diameter:min	13.5 millimeters	0.531 in
nom	13.7 millimeters	0.539 in
max	14.1 millimeters	0.555 in
Area	1.131 cm^2	0.175 in^2
Yield Strength*	190 kN	42.7 kips
Tensile Strength	210 kN	47.2 kips
Min. Elongation	4.5%	4.5%

*Load at 0.2% elongation

Given the properties and arrangement of the tendons, the tensioning forces were specified to achieve the same effect in the model as the prototype, considering the unique features of the model prestressing system that do not scale. Three basic criteria were used to establish equivalence between the prototype and model prestressing.

1. First, the state of prestressing in the model should reflect the predicted state of stress in the prototype after reaching its 40-year design life. Since the model was tested approximately six months after tensioning the tendons, it was necessary to adjust the initial tensioning forces to account for the expected creep and relaxation losses in the prototype.
2. Second, the effective hoop compressive stress due to prestressing should be the same in the model as the prototype. This relates directly to the requirement that the hoop tensile response and failure mode in the cylinder wall be accurately modeled.
3. Third, the vertical compressive stress in the concrete at the base of the cylinder wall should be the same in the model and the prototype. This relates directly to the requirement that the bending/shear response and failure mode at the base of the cylinder wall be accurately modeled.

Given these criteria, the following factors were considered:

1. Tendon friction: Tendon stresses decrease from the point where the tension load is applied, i.e., the anchor, due to friction between the tendon and the sheath and between the strands themselves. Two components of friction are considered in the design; 'wobble' friction, λ, which results from the internal friction between the tendon strands and ducts, and angular friction, μ, which occurs as a result of sweeping the tendons around a curve. The tendon stress at any point, σ_x, along the length of the tendon is given by:

$$\sigma_x = \sigma_o e^{-(\mu\alpha + \lambda l)}$$

where σ_o is the applied tension, α is the arc length, and l is the distance from the anchor along the tendon.

The values of μ and λ used in the design of the prototype were 0.14 and 0.001, respectively. Since the model strands were actually larger in diameter than those used in the prototype (and therefore stiffer) and bent to a '4x' tighter radius, tests of the model tendons resulted in values for angular and wobble friction coefficients of

$$\mu = 0.21, \lambda = 0.001$$

2. Setting Losses: After the tendons are tensioned, the tensioning forces are locked in by seating the strands in the anchor blocks using tapered wedges. During this process, there is some loss of anchor force due to slipping and settling of the anchor components. The tensioning hardware (anchors, wedges, jacks, etc.) cannot be scaled and as a result, the maximum setting loss specified for the model, 5 mm (0.2"), is larger than the scaled setting loss and nearly equal to the actual setting loss specified for the prototype. (The setting loss, specified in terms of length, is the measured change in length of the projecting tails of the tendons strands before and after anchoring.)

The larger setting loss, coupled with the higher friction coefficients for the model, result in stress profiles in the model tendons that are much less uniform than those in the prototype.

3. Gravity: For geometric scaling, mass densities are not scaled correctly if the same materials are used to construct the model and the prototype. For static tests, this only affects the dead load stresses, which, typically, are only a small percentage of the total stress. For the static overpressurization tests of the PCCV, this scaling artifact would not significantly affect on the model response, except, possibly, at the wall-base junction. Compressive stresses due to dead load are larger at the base of the cylinder wall than anywhere else in the model, and this stress may be an important response component for a bending/shear failure mode. Consequently, vertical tendon design loads were increased in the PCCV model to compensate for the reduced stress due to dead load at the wall-base junction.

The final tendon design stress profiles are shown in Figure 2.9. The profiles are given for a typical hoop tendon in the cylinder wall and for the longest and shortest vertical hairpin tendons. The stress distribution for the shorter hoop tendons in the dome and for both hoop and vertical tendons deflected around penetrations are not shown but can be calculated in a similar manner. (Note that the design tensioning and anchor forces for 'deflected' tendons are not adjusted in either the prototype or the model, to account for additional friction losses due to 'in-plane' curvature.) The corresponding design anchor forces are given in Table 2.5. These values were included in the model prestressing specifications. The as-built prestressing results are summarized in Section 2.2.3.

Table 2.5 PCCV Model Design Prestressing Anchor Forces

Tendons	Tensioning Force	Lift-Off Force	Losses (Creep and Relaxation)*	At Test
Vertical Tendons	49.6 tonnes (109.3 kips)	46.3 (102.1)	3.1 (6.8)	43.2 (95.3)
Hoop Tendons	44.4 tonnes (97.9 kips)	34.1 (75.2)	3.1 (6.8)	31 -68.4

*Losses evaluated at six months.

Considering the design tendon stress profiles, the prestressing design criteria can be satisfied. For the prototype, the average hoop tendon stress after 40 years is 85.3 kg_f/mm^2 (121.3 ksi). Calculating the equivalent pressure, p_{eqv}:

$$p_{eqv} = \frac{\sigma a}{R s} = \frac{(85.3\ kg_f/mm^2)(5429\ mm^2)}{(2150\ cm)(45\ cm)} = 4.8\ kg_f/cm^2\ (68\ psi)$$

where

a = the area of the tendon,
R = the inside radius of the containment, and
s = the hoop tendon spacing.

For the model, the average hoop stress after six months is 85.7 kg_f/mm^2 (121.8 ksi) and the equivalent pressure is:

$$p_{eqv} = \frac{\sigma a}{R s} = \frac{(85.7\ kg_f/mm^2)(339.3\ mm^2)}{(537.5\ cm)(11.25\ cm)} = 4.8\ kg_f/cm^2\ (68\ psi)$$

which is essentially identical to the prototype. Comparing the design pressure, P_d, the hoop prestressing is equivalent to applying a counterbalancing pressure of 120% of the design pressure.

$$\frac{P_{eqv}}{P_d} = \frac{4.8 kg_f/cm^2}{4.0 kg_f/cm^2} = 1.20$$

Comparing the concrete compressive stress at the base of the wall:

For the prototype after 40 years:

$$\sigma_c = \frac{\sigma a}{t s} = \frac{(106.3\ kg_f/mm^2)(5429\ mm^2)}{(130\ cm)(77.32\ cm)} = 57.4\ kg_f/cm^2\ (817\ psi)$$

Concrete compressive stress due to Dead Load 15.2 kg_f/cm^2 (216 psi)

Total compressive stress in Concrete 72.6 kg_f/cm^2 (1,033 psi)

where t is the thickness of the containment wall and s is the vertical tendon spacing.

For the model after 6 months:

$$\sigma_c = \frac{\sigma a}{t s} = \frac{(127.5\ kg_f/mm^2)(339.3\ mm^2)}{(32.5\ cm)(19.33\ cm)} = 68.9\ kg_f/cm^2\ (980\ psi)$$

Concrete compressive stress due to dead load 3.2 kg_f/cm^2 (46 psi)

Total compressive stress in concrete 72.1 kg_f/cm^2 (1025 psi)

Therefore, the higher vertical tendon stress in the model, when combined with the dead load stress, yields nearly the same compressive stress in the concrete as the prototype.

2.2 Construction

2.2.1 General Construction

Prior to construction of the PCCV model, during the initial development of the containment test site in 1993, the location of the PCCV model was selected, the surface soil was removed, and the existing subgrade was excavated to a depth of over 8 m (25') and replaced with a compacted engineered backfill. The allowable bearing capacity, based on limiting soil settlement to 25 mm (1") or less, is 3.11 kN/m^2 (6.5 ksf) [26].

The overall site plan was shown in Figure 1.3. A detail of the areas surrounding the PCCV model is shown in Figure 2.10. The model was oriented so the E/H opening was facing due south. (This was primarily for operational considerations rather than any test requirement.) An aerial view of the test site during construction is shown in Figure 2.11.

On-site construction of the model by Hensel Phelps Construction Co. commenced on January 3, 1997 with construction of a 19.8 m × 19.8 m × 30 centimeters thick (65' × 65' × 1') mudmat placed on the engineered back-fill (Figure 2.12). This mudmat was constructed of 'lean' concrete and reinforced with welded wire fabric to provide a level working surface on which to construct the model. Benchmark monuments were constructed of small concrete pads at each of the four cardinal azimuths (0 degrees, 90 degrees, 180 degrees, and 270 degrees) outside the perimeter of the construction zone. These control points were subsequently used for the model's layout.

After the mudmat concrete had cured, a steel frame to support the basemat rebar was erected (Figure 2.13) and the rebar for the first basemat lift (F1) was erected (Figure 2.14). After verifying the position of the rebar (Figure 2.15), the formwork was set (Figure 2.16) and the F1 concrete placed (Figure 2.17). While F1 concrete was placed directly on the mudmat, there was no positive connection between the two.

Most of the model reinforcing was prefabricated by Border Steel Co., El Paso, TX, although some field fabrication was required as the construction progressed. All concrete was batched by Lafarge Construction Materials (formerly doing business as Western Mobile NM), Albuquerque, NM, mixed in transit and placed by pumping. All sampling and quality control tests were conducted by AGRA Earth and Environmental, Inc., Albuquerque, NM. Slump (Figure 2.18) and air entrainment tests were conducted on each batch/truck of concrete delivered to the site and standard cylinders and beams

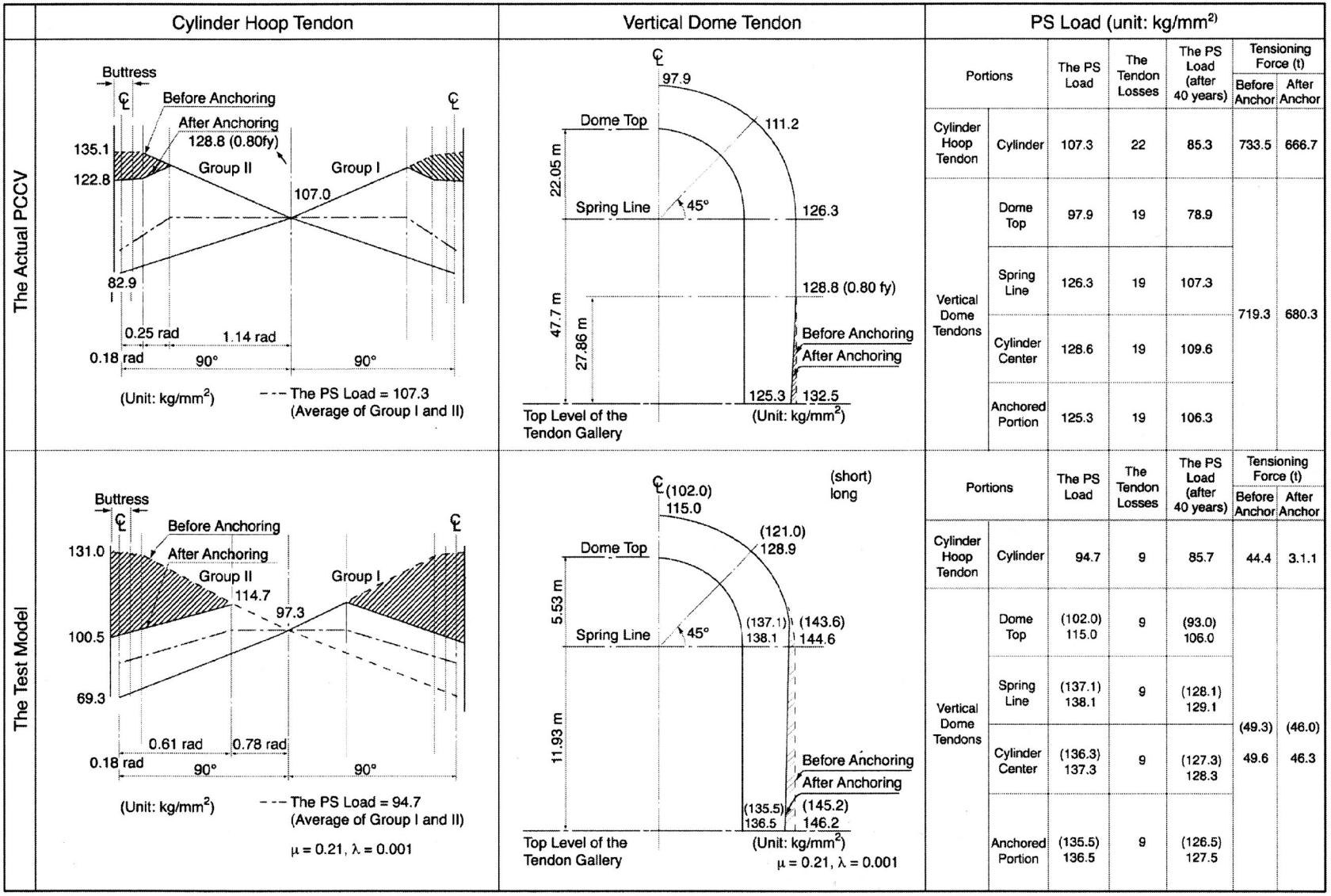

PS Load (unit: kg/mm²)

Portions		The PS Load	The Tendon Losses	The PS Load (after 40 years)	Tensioning Force (t) Before Anchor	Tensioning Force (t) After Anchor
Cylinder Hoop Tendon	Cylinder	107.3	22	85.3	733.5	666.7
Vertical Dome Tendons	Dome Top	97.9	19	78.9	719.3	680.3
	Spring Line	126.3	19	107.3		
	Cylinder Center	128.6	19	109.6		
	Anchored Portion	125.3	19	106.3		

Portions		The PS Load	The Tendon Losses	The PS Load (after 40 years)	Tensioning Force (t) Before Anchor	Tensioning Force (t) After Anchor
Cylinder Hoop Tendon	Cylinder	94.7	9	85.7	44.4	3.1.1
Vertical Dome Tendons	Dome Top	(102.0) 115.0	9	(93.0) 106.0	(49.3) 49.6	(46.0) 46.3
	Spring Line	(137.1) 138.1	9	(128.1) 129.1		
	Cylinder Center	(136.3) 137.3	9	(127.3) 128.3		
	Anchored Portion	(135.5) 136.5	9	(126.5) 127.5		

Figure 2.9 PCCV Prototype and Model Tendon Design Stress Profiles

were cast (Figure 2.19) for testing at seven, 28, and 91 days and at the time of tensioning and pressure testing. Both standard-cure, SC, (two to four days in a water bath, then stored in a humidity controlled chamber until testing), and field-cured (FC) specimens (two to seven days in a water bath, then stored on-site until testing) were produced and tested.

Installation of rebar and concrete placement for F2, F3, and F4 followed a similar sequence (Figures 2.20-2.25). Strain gages and thermocouples (T/Cs) were mounted on some of the rebar prior to installation and the lead wires were routed through the forms prior to concrete placement. As noted previously, the concrete outside the tendon gallery was not placed, thus allowing access for insertion and tensioning of the vertical tendons. The bottom basemat rebar that extended beyond the initial basemat lifts was covered with a temporary plywood deck to protect it from damage during construction until the final basemat pours (F5 and F6) were made. Other rebar that extended beyond lifts F1 to F4 were terminated and equipped with mechanical splices.

Prior to construction of the cylinder wall, a mock-up of the wall, incorporating the E/H embossment, vertical buttress, tendon sheaths, and the liner, was constructed to develop and demonstrate the erection sequence and method for placing the cylinder wall concrete (Figure 2.26). Since the wall lifts were approximately 3 m (10') in height, form 'windows' were located at mid-height (Figure 2.27) to limit the drop height of the wet concrete. Due to the dense rebar pattern, the trunk of the concrete pump could not be inserted into the forms. After placing the concrete through the form window and using spud-type vibrators to consolidate the concrete and prevent voids, the windows were blocked and placement of concrete continued at the top of the mock-up. After the concrete had cured and the exterior form was removed, the mock-up was cored to inspect for voids in the concrete. None were discovered. While this sequence of construction was not completely identical to the sequence for the model wall (e.g. continuing vertical wall reinforcing would limit placement at the top of each lift), the mock-up demonstrated that the planned construction sequence would be successful.

Since New Mexico is subject to severe summer lightning storms and the PCCV model is in an exposed desert terrain, a lightning protection system, consisting of four 30 m (100') poles connected to a buried copper cable counterpoise, was installed around the model. The lightning protection system provides an alternate path to ground around the model, thereby preventing direct lightning strikes that might damage the instruments, wires, and data acquisition components. Until the dome was completed, only two of the poles at 0 degrees and 180 degrees could be installed to accommodate crane operations, thereby providing only partial protection. Nevertheless, the protection system appears to have functioned successfully, since no direct lightning strikes were ever recorded on the model, even though there was a strike on the chain-link fence surrounding the site that damaged unprotected telephone lines strung along the fence.

While the basemat and wall mock-up construction was being completed, the liner panels, which had been fabricated by MHI in Kobe, Japan, were shipped to the test site. The liner panels arrived at the site in June, 1997 (Figure 2.28). Prior to shipping the panels to the U.S., all the cylinder wall panels were temporarily erected in Kobe to ensure that they would fit. Typical liner panels with support jigs are shown in Figure 2.29.

At the same time the liner panels were being shipped, an internal structural steel frame was fabricated (in the U.S.) and also delivered to the test site. This structure, known as the instrumentation frame, provided the support structure from which to hang the liner panels, with jigs, prior to welding; provided internal support during concrete placement; and provided a work platform during liner welding and installation of the internal instrumentation. During testing, this internal frame also acted as the reference structure for measuring model displacements. Components and erection of the instrumentation frame are shown in Figures 2.30-2.33.

Beginning in September, 1997, the liner panels were erected and bolted to the frame (Figures 2.34-2.36). After all the panels were assembled, a crew of welders from MHI began welding the liner seams. First, the basemat liner plates were welded to the embedded anchors. The liner erection plan then called for the seam between the first liner ring and the basemat to be welded, followed by the horizontal seam between the first and second liner rings. After this, the vertical seams for the first ring were completed. The liner erection and welding specifications defined overall and local dimensional tolerances and nondestructive inspection criteria. All liner welds were radiographed and inspected for flaws (undercutting, inclusions, and porosity). Initial difficulties welding the 1.6 mm liner in the field resulted in most of first ring's liner welds is being rejected. These welds were then ground out and repair welds were made. While there was some improvement, some of the repair welds contained flaws that exceeded the welding specifications. After additional repairs, inspection, and laboratory tests of welded liner specimens, it was decided that the original welding specifications were overly conservative and the criteria on flaws were relaxed. (The original weld flaw acceptance criteria had been scaled from the prototype welding specifications.)

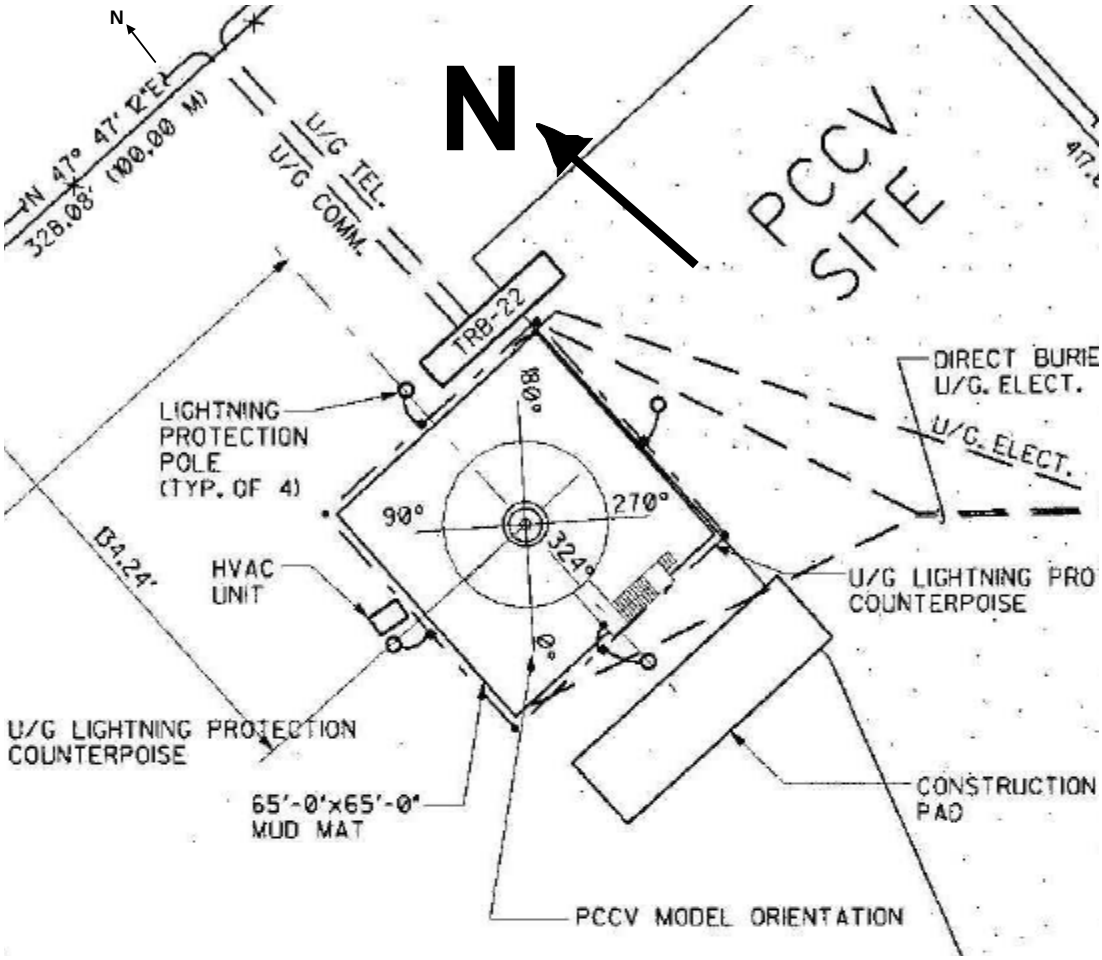

Figure 2.10 PCCV Model Layout

For the 6.4 mm (1/4") thick liner in the prototype, the liner seam welds could be made using double-sided full penetration welds. However, this method of welding could not be used for the 1.6 mm (1/16") thick model liner welds. The field welds in the model liner required back-up bars or, in some locations, back-up tape, and the full penetration welds were made from one side. Where welds were ground out and repaired, it was sometimes necessary to remove a section of the back-up bar and replace it with another segment. (Note that this created some local discontinuities in the model liner that became important during the pressure tests, but which were not representative of details in the prototype.) In areas where liner strains were expected to be high due to geometric discontinuities, the back-up bars were removed after the liner welds were completed to maintain the similarity with the prototype. In some locations, the weld bead was ground to reduce its profile, as well.

Both of these cosmetic post-weld treatments may have caused local thinning of the liner. Unfortunately, no measurements of the post-weld liner thickness were made. After the liner seam welds were completed, the penetration insert assemblies were welded to the liner and the stiffener, and liner anchor welds were completed.

To expedite the liner strain gage installation and the model's erection, a number of strain gages on the exterior surface of the liner, i.e. the concrete side of the liner, were installed prior to erection and welding of the liner panels. Since heat input from the welding operations could damage strain gages near the weld seams, only those gages over 10 cm (4") from the weld seams were installed prior to erection. This included gages on the liner anchors and stiffeners. Figure 2.36 shows two liner panels during installation of the strain gages. After the liner panels were erected and welded, the exterior

Figure 2.11 Aerial View of CTTF-West during PCCV Construction (March, 1999)

strain gages near the liner weld seams were installed. Figures 2.38 and 2.39 show typical strain gage installations near weld seams.

After all weld inspection criteria had been satisfied, construction of the model proceeded with the installation of inner horizontal and vertical rebar layers in the cylinder and dome (Figures 2.40-2.41). All instrumented rebar for these two layers was installed concurrently with the remainder of the reinforcing steel.

Next, the tendon sheath support frame, consisting of steel angles with support pins to correctly position the tendon sheaths, was installed (Figure 2.42). Except for the instrumented hoop tendons, which were preassembled with the sheath, all the tendon sheaths were all installed prior to outer reinforcing and shear reinforcing (Figures 2.43 and 2.44). The model construction then proceeded by lifts; C1 through C4 in the cylinder, and D1 to D3 in the dome. For each lift, the outer and radial rebar, including instrumented rebar and any instrumented hoop tendons, were installed first. Lead wires for the liner, rebar and tendon strain gages, embedded T/Cs, and fiber optic strain gages, were then routed through PVC ducts that had been placed in the previous lift. After checking that the gages and lead wires had not been damaged and were still functioning, the outer concrete forms were installed and concrete for each lift was placed. After the concrete had cured sufficiently, the outer forms were stripped and the cycle was repeated until the final dome pour was completed. The final dome pour, D3, was completed without the use of external forms. The plasticizer was not added for this lift, so a low slump was maintained and the final surface was hand finished, aided by a wooden template that defined the outer surface. This sequence of construction is illustrated in Figures 2.45 through 2.52.

After the D3 concrete achieved its specified strength, the liner jigs were cut loose from the liner, detached from the interior frame, and removed. This freed the containment wall from the interior frame, making both structures independent of each other. The instrumentation frame then functioned as a work platform and as the reference frame for measuring shell displacements.

After the liner jigs were removed, model construction was temporarily suspended while SNL assumed control of the model for installing of the interior instrumentation. Details of the instrumentation installation are provided in Chapter 3. Prior to installing the interior instrumentation, the interior of the liner surface was cleaned and painted white. Cardinal lines were surveyed and marked on the liner as reference for the installation of the interior instrumentation. The as-built radii at the intersections of the cardinal lines were also determined, and the results are tabulated in Appendix C.

Prior to beginning the interior instrumentation, interior lighting, power, and ventilation were installed. Structural steel stairs to the top of the basemat and E/H were erected, and a vestibule with locking doors for access control was installed over the E/H opening. Machined flange covers were installed over the M/S and F/W penetration sleeves. Six of these covers were drilled for the sealed instrumentation feedthroughs and the remaining two were equipped for the power feedthrough and the pressurization line.

While the interior instrumentation was completed, construction activities resumed after an approximately six-month hiatus with the insertion of prestressing tendons into the sheaths. After the interior instrumentation was completed and verified ready for operation, the DAS was started prior to tensioning the tendons. Details of the prestressing operations and results are described in Section 2.2.3. After prestressing was completed, model construction concluded with the placement of the final basemat concrete lifts, F5 and F6 (Figure 2.53). After the forms were stripped, Mitsubishi and Hensel Phelps demobilized and turned the model over to SNL on July 28, 2000. The completed PCCV model is shown in Figure 2.54.

2.2.2 Material Properties

Properties of all the PCCV model construction materials, except for the model concrete, were determined from tests prior to construction and summarized in Section 2.1. Model concrete properties were determined by testing standard specimens (cylinders and beams) cast during placement of each concrete lift.

All concrete testing was conducted according to ASTM standards[10] and the results are summarized in Appendix B. Quality control tests, consisting of standard 6-inch cylinder, unconfined compressive strength tests, were performed by AGRA Earth and Environmental, Inc. Specimens were cast from nearly every truck of concrete placed in the model. (Each truck contained approximately 7.6 m^3 (10 cubic yards.)) Standard Cured (SC) specimens were cured in a water bath for two to four days (depending on weekends) and stored in a humidity-controlled chamber until tested. FC specimens were also cured in a water bath for two to four days, then stored at the site, under blankets, until tested. Compression tests[11] of both SC and FC cylinders were conducted at seven, 28, and 91 days. 91-day strengths were compared to the specified design strengths.

The average 91-day FC strength results for the first two cylinder wall lifts, C1 = 389kg_f/cm^2 (5527 psi) and C2 = 436kg_f/cm^2 (6200 psi), failed to meet the minimum specified design strength of 450 kg_f/cm^2 (6400 psi). This may have resulted from cold weather conditions, which might have retarded the curing rate. Analysis of the test data suggested that the concrete would reach the specified minimum design strength by the time prestressing was scheduled to occur, so no action was deemed necessary. Nevertheless, the curing method of FC specimens for lifts C4 through D3 and F5 and F6 was modified to keep the cylinders in the water bath for seven days. This modified field curing method is designated FC' in the material data summary.

While the strength of the concrete in C1 and C2 was deemed adequate, there was a concern that the low strength might cause higher creep losses than anticipated in the prestressing design calculations. Creep tests[12] of two specimens each from C1 and C2 were conducted at the University of New Mexico and compared to the results of the trial mix creep tests

[10] *Annual Book of ASTM Standards*, American Society for Testing and Materials (ASTM), Philadelphia, PA.
[11] ASTM C39-94, "Standard Test Method for Compressive Strength of Cylindrical Concrete Specimens."
[12] ASTM C512-87, "Standard Test Method for Creep of Concrete in Compression" (modified).

Figure 2.12 Placement of PCCV Mudmat

Figure 2.13 Basemat Rebar Support Frame

Figure 2.14 Basemat Bottom Bars and Vertical Ties

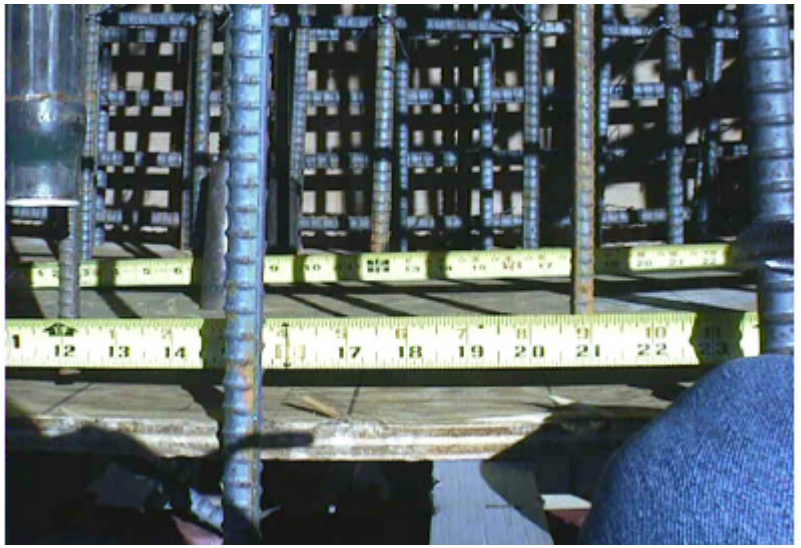

Figure 2.15 Measuring Rebar Location

Figure 2.16 F1 Formwork

Figure 2.17 Placing F1 Concrete

Figure 2.18 Measuring Concrete Slump

Figure 2.19 Concrete Test Cylinders and Beams

Figure 2.20 F2 Rebar Erection

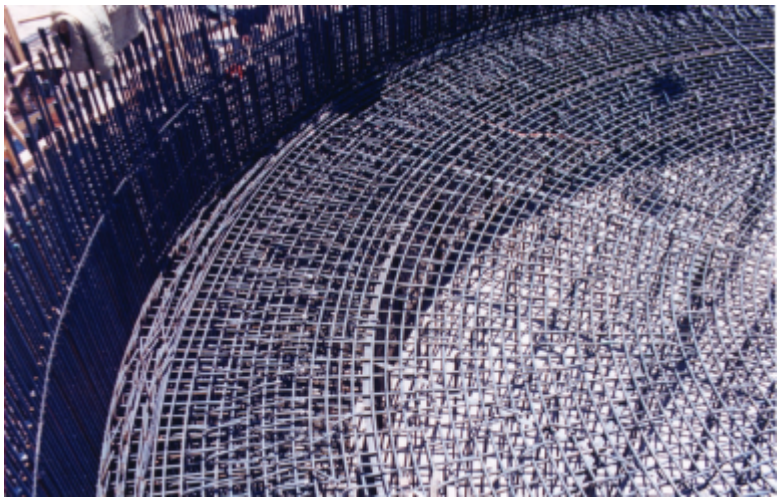

Figure 2.21 F3 Rebar

Figure 2.22 F3 Rebar and Formwork

Figure 2.23 Basemat Top Rebar (F3) and Wall Dowels

Figure 2.24 F3 Concrete Placement

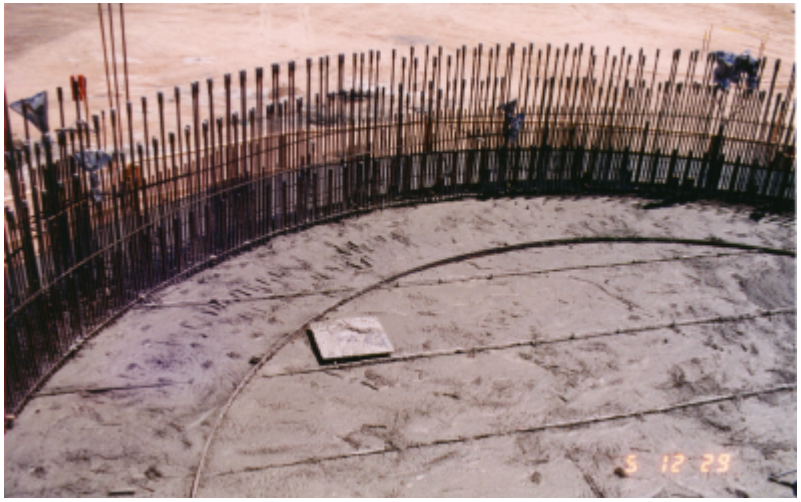

Figure 2.25 F4 Concrete

Figure 2.26 Wall Mock-Up Rebar

Figure 2.27 Wall Mock-up Form w/ Concrete 'Window'

Figure 2.28 Delivery of Liner Panels

Figure 2.29 Liner Panels after 'Uncrating'

Figure 2.30 Instrumentation Frame Column 'Trees'

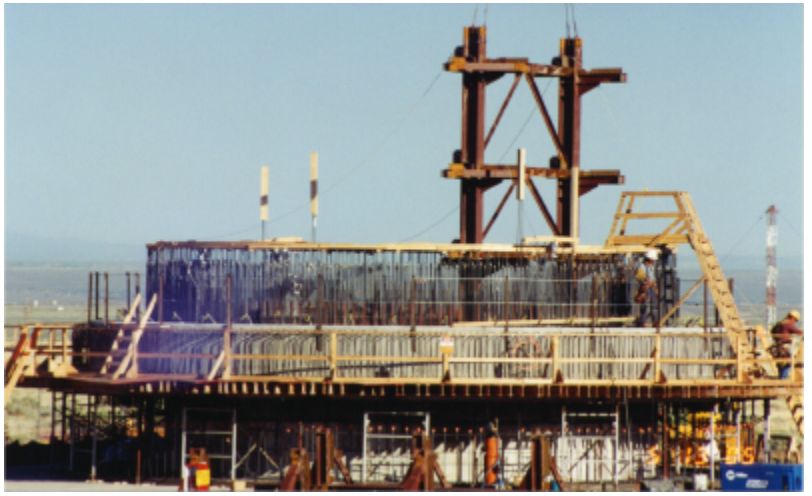

Figure 2.31 Instrumentation Frame Erection

Figure 2.32 Instrument Frame Erection

Figure 2.33 Completed Instrument Frame

Figure 2.34 Liner Panel Erection

Figure 2.35 Dome Liner Erection

Figure 2.36 Liner Panels with Jigs

Figure 2.37 Liner Panel Instrumentation

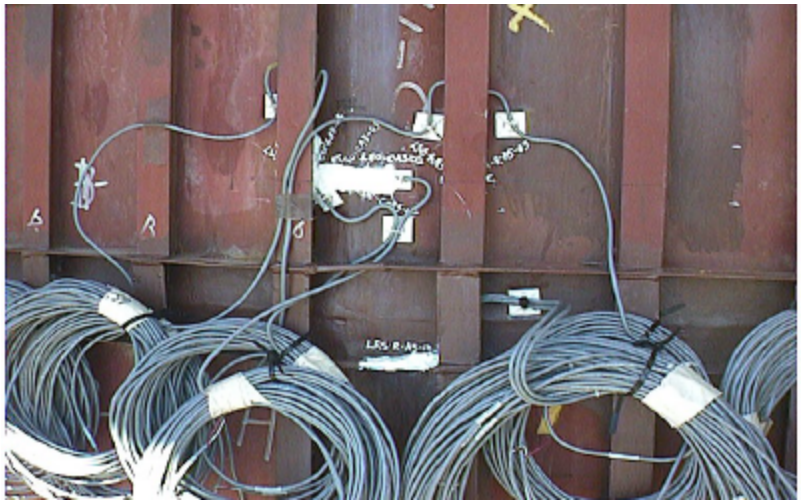

Figure 2.38 Liner Strain Gages after Welding

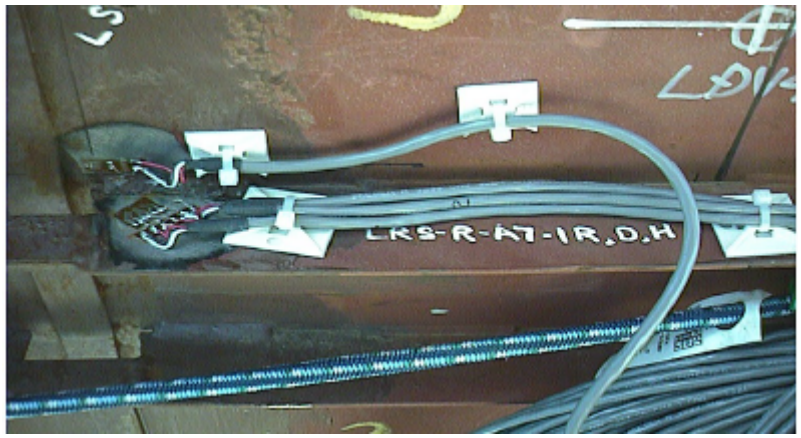

Figure 2.39 Close-Up of Liner Strain Gages near Weld

Figure 2.40 Inner Rebar at M/S Penetrations

Figure 2.41 Installation of Inner Dome Rebar

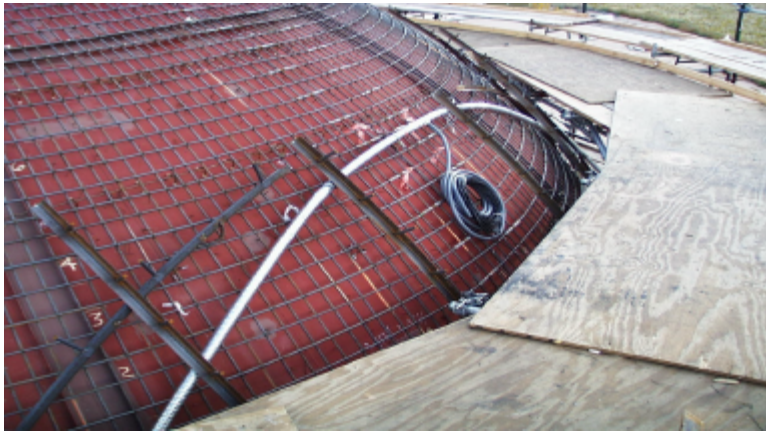

Figure 2.42 Tendon Sheath Support Frame

Figure 2.43 Dome Tendon Sheaths and Support Frame

Figure 2.44 PCCV Model Tendon Sheaths

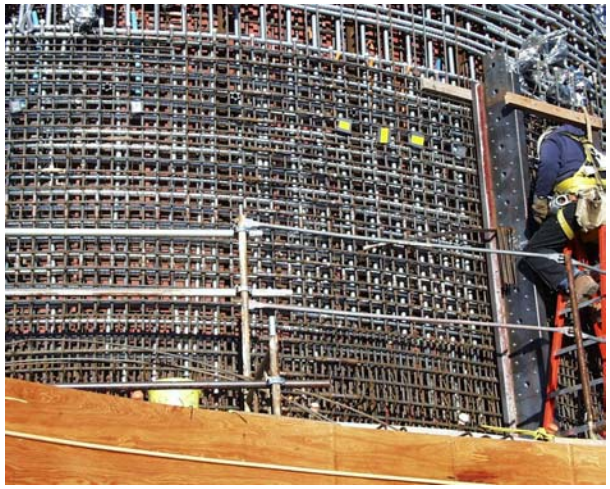

Figure 2.45 Outer Rebar for C1

Figure 2.46 C1 Formwork Installation

Figure 2.47 Placing C1 Concrete

Figure 2.48 Installation of Instrumented Hoop Tendon.

Figure 2.49 C2 Formwork

Figure 2.50 C4 Concrete Placement

Figure 2.51 D1 Formwork Erection

Figure 2.52 D3 Concrete Placement

Figure 2.53 Final Basemat Concrete Lifts

[27]. These results, presented in Appendix B, showed higher amounts of creep and shrinkage than the trial mix data and indicated that creep losses in the prestressing might be higher than expected. This data was considered in specifying the tensioning forces for the tendons in Table 2.5.

More extensive material property tests for FC specimens were conducted around the time the model was being tensioned and just prior to the Limit State Test (LST). These tests provided more accurate material property data for concrete constitutive models used in the pre- and posttest analyses to predict and simulate the model response to pressure. These tests were also conducted at the University of New Mexico and included unconfined compression tests, compression tests to determine modulus of elasticity and Poisson's ratio[13], split cylinder tensile strength[14], and modulus of rupture[15]. The unit weight of the specimens was also determined and, since prediction of concrete cracking was one of the pretest analysis milestone objectives, a limited number of direct tension tests were conducted on specimens from the cylinder wall. The results of these tests and the direct tension test procedure are detailed in Reference [28] and summarized in Appendix B. A summary is also provided in Table 2.6.

A few other observations on the model concrete are worth noting:

1. The Coefficient of Variation (COV) in the compressive strength of the FC model concrete was 15.9% at 91-days and 13% at the time of prestressing. This COV is larger than typically observed for concrete from a central batch plant and indicates a significant degree of variation in the model concrete properties.

2. Compressive failure strains in the concrete specimens were typically in the range of 0.25 to 0.30%. While the tensile failure strain was not determined, the direct tension tests performed by the University yielded critical crack opening displacement data, which could be utilized in a fracture mechanics approach.

3. The modulus of elasticity in compression, determined from test data, is significantly lower than values usually computed from 'rules-of-thumb.' For example, ACI 318[16] recommends that $E_c = 57{,}000\ \sqrt{f_c'}$ in psi. Using 9300 psi as the average strength of the field cured cylinder/dome specimens yields an elastic modulus of 5.51×10^6 psi, compared to the measured value of 3.90×10^6 psi, a reduction of nearly 30%. If the modulus were based on the specified minimum strength of 6400 psi, the resulting value would be 4.56×10^6 psi, still higher than the measured value by 15%.

---

[13] ASTM C469-94, "Standard Test Method for Static Modulus of Elasticity and Poisson's Ratio of Concrete in Compression."

[14] ASTM 496-96, "Standard Test Method for Splitting Tensile Strength of Cylindrical Concrete Specimens."

[15] ASTM C78-94, "Standard Test Method for Flexural Strength of Concrete (Using Simple Beam with Third-Point Loading)."

[16] *Building Code Requirements for Structural Concrete,* ACI 318-02, American Concrete Institute, Farmington Hills, MI.

Figure 2.54 Completed PCCV Model

2.2.3 Prestressing Operations

With the majority of the model instrumentation suite installed, model construction resumed in February, 2000 with the insertion of noninstrumented tendon strands into the sheaths embedded in the model. Prior to insertion, the strands were coated with an anti-corrosive agent, but there was no other treatment. Insertion was achieved by feeding a 'puller cable' through the sheath equipped with a wire gripping sleeve that tightened on the strands as it was tensioned to pull them through the sheath (Figure 2.55). Except for a few minor obstacles, e.g. grout which had penetrated the sheath splices and had to be cleared, the sheaths were clear and insertion was accomplished without any difficulty.

Table 2.6 PCCV Model Average Concrete Properties

Design Compressive Strength		**300kg$_f$/cm^2**	**(4300 psi)**	**450kg$_f$/cm^2**	**(6400 psi)**
@ Prestressing					
Compressive Strength,	FC	570	(8102)	559	(7956)
	FC'	NA	NA	680	(9665)
Young's Modulus		25.7 GPa	(3.7×10^6 psi)	27.2 GPa	(4.0×10^6 psi)
@ Limit State Test					
Compressive Strength,	FC	562	(7998)	615	(8750)
	FC'	NA	NA	700	(9953)
Young's Modulus		27.2 GPa	(3.9×10^6 psi)	26.9 GPa	(3.9×10^6 psi)
Poisson's Ratio		0.21		0.22	
Split Tensile Strength		35	(497)	36	(519)
Direct Tensile Strength		NA	NA	23	(320)
Modulus of Rupture		NA	NA	42	(594)
Density		2186kg$_f$/m^3	(136.4 pcf)	2176kg$_f$/m^3	(135.8 pcf)

The suite of gages installed on the model prior to prestressing and installing the DAS cleared the final system checks, and the DAS was put into operation at 11:48 AM, March, 3, 2000. The initial data scan represented the initial or 'zero' reading for all the model transducers. All subsequent readings, through the LST until the DAS was shut down in October, are referenced to this initial scan. The model was scanned hourly for seven days to provide baseline information on the response to ambient temperature variations prior to tensioning the model and to verify the operational readiness of the DAS in attended and unattended modes.

Model prestressing began on March 10, 2000. The arrangement of the model tendons is shown in Appendix A. The nomenclature for identifying individual tendons consisted of an alpha designator 'H' for hoop tendons and 'V' for vertical tendons, followed by a numerical designator (1 through 98 for the hoop tendons and 1 through 90 for the vertical tendons). The hoop tendons were numbered consecutively from 1, the lowest tendon in the cylinder wall, to 98, at the midpoint of the dome. Even-numbered hoop tendons (H2, H4, H6,…, H98) were anchored at the 90 degree buttress and odd-numbered hoop tendons (H1, H3,…, H97) were anchored at the 270 degree buttress. Vertical tendons were numbered consecutively from V1 at 45 degrees, clockwise to V90 at 223 degrees. The vertical tendons were arranged in two orthogonal groups, with V1 through V45 spanning the dome in a plane (nearly) parallel to the 90 to 270 degree axis and V46 through V90 in an orthogonal plane approximately 0 to 180 degrees. This arrangement is illustrated more clearly in the design drawings and shown in Figure 2.44.

Figure 2.55 Pulling Hoop Tendons

Prestressing operations were defined by MHI in the project construction specifications[17]. The overall sequence of tensioning is illustrated in Figure 2.56. This sequence is identical to that used for the prototype and is intended to apply balanced prestressing forces to the model to prevent excessive local deformation or damage. The actual tensioning schedule is shown in Table 2.7. Prestressing operations were completed on May 3, 2000.

Thirty-four of the 188 tendons were instrumented with load cells at the anchors, and eight of these tendons, five hoop and three vertical, were also instrumented with strain gages at discrete locations along their length in an attempt to monitor and record the force distribution for comparison with the design calculations. The instrumented tendons are identified in Table 2.7 and their locations are illustrated in Figure 3.21. Details of the tendon instrumentation are given in Chapter 3.

Only one tendon was tensioned at a time (Figure 2.56). The procedure was to assemble the tensioning hardware at each end of the tendon. The tensioning hardware consisted of the tendon anchor and wedges, tensioning chair, hydraulic jack, and tensioning anchor. For the instrumented tendons, a pair of bearing plates, spherical washers, and the load cell was inserted between the tendon anchor and the bearing plate embedded in the model. This arrangement is shown in Figure 2.58. After the tensioning hardware was assembled, one end of the tendon, designated the 'B' end, was tensioned to 10% of the design load while the jack on the 'A' end was locked off. Then the B-end jack was locked off and the tensioning force was applied continuously by the jack at the A end until the jack pressure gage indicated that the force specified in Table 2.5 had been reached. (The jacks were calibrated prior to the start of prestressing and the conversion between hydraulic pressure and force was established for each jack.) In most cases, the tendon 'stretch' exceeded the maximum stroke of the jack and the strands had to be regripped to complete tensioning. When the A end was at the maximum load, the force at the B end was recorded and the friction coefficients for the tendon were computed and compared to the design values. (If the friction deviated from the design values by more than a specified range, the tendon was retensioned or, in some instances, the tendon was removed and new strands were inserted.) The B end was then tensioned to the specified force. When both ends were at the specified force, the anchors were seated.

[17] MH-K10-29, "Prestressing Work Procedure," Rev. 1, Mitsubishi Heavy Industries, May, 1999.

The seating loss, defined in terms of length, was measured as the difference between the length of the tendon extending beyond the anchor, before and after seating. This indicates the loss of elongation (and hence tension) in the tendon as the load is transferred from the jack grips to the tendon anchors. The measured seating loss was compared to the maximum design seating loss of 5 mm (0.2"), and, if it was excessive, the tendon was retensioned. After seating the tendon, each end was subjected to a 'lift-off' test in which the tendons were regripped and pulled until the tendon anchor lifted off the bearing plate enough to insert a feeler gage between them. The measured lift-off force was also compared to the value specified in Table 2.5.

The instrumented tendons, those with load cells only and those with strain gages, were closely monitored during tensioning but the load cell data was not reported to the tensioning contractor, VStructural, LLC., during prestressing. The tensioning procedure was modified for the eight instrumented tendons with strain gages. Since the lead wires for these gages would be damaged if the tendon was pulled in one direction first and then the other, causing the gages and the lead wires to travel back and forth in the sheath, these tendon were tensioned simultaneously at both the A and B ends. The tensioning forces were applied in small load increments and the tendon gages were monitored continuously during tensioning. The responses of the instrumented tendons are shown as force time histories in Figures 2.59 through 2.66.

These figures show the response of the load cells at each end of the tendons and the response of the surviving strain gages (converted to force by multiplying the strain by the nominal tendon area and elastic modulus of the strand). The strain gages on these tendons suffered a high mortality rate during prestressing, as shown in Table 2.8. Nevertheless, a high mortality rate was expected, and in most cases the surviving strain gages provided insight into the behavior of the tendons during prestressing and subsequent pressure testing.

The figures illustrate the range of strain in individual strand wires at a given measurement position, and also show when some of the strain gages failed. The data was not plotted after a gage had failed. It is interesting to note that the Tensmeg gages (TT) typically gave lower strain readings than the bonded foil gages (TF) mounted on individual wire strands. This is likely due to the Tensmeg end blocks slipping relative to the strand, resulting in an inaccurate measure of the strand strain. For most future discussions of the tendon response, only the data from the TF gages is considered as a reliable measure of the tendon strain and the TT data is ignored.

Figure 2.62 illustrates how the stages of the prestressing procedure are reflected in the test data. In the figure for H67, the surviving strain gages at each measurement position along the length of the tendon were averaged before converting them to a tendon force. This was done to simplify the plot, but this also recognizes that the force in individual wires in the tendon strands vary and the load cells (TL) forces and average forces from the strain gages (TF or TT) are plotted as a function of time. The force time history shows the load being applied incrementally at both ends of the tendon until the specified tensioning force was achieved and load was stable. Note that at a force of approximately 30T, the tendon was anchored and regripped when the stroke of the jacks was exceeded. After stabilizing at the maximum force, the tendons were seated, with the corresponding drop in load at and near the anchors. The slight increase in force at the anchors after seating reflects the lift-off test. (This shows that the force required to lift-off the anchor is slightly higher than the seated anchor force.)

Note also that the strain gages were most likely to fail near the tendon anchors and less likely to fail at the tendon mid-point. This occurs because the strands near the anchors travel the furthest during tensioning, increasing the likelihood that the gages or their lead wires were crushed against the sheath wall or another strand.

Considering Figure 2.62, it can be seen that the general force distribution along the length of the tendons is consistent with the design assumption, i.e., the highest tendon force is near the anchor and the lowest force is at the mid-point of the tendon. Figures 2.67 through 2.74 compare the measured force distribution in the tendons during and after tensioning with the design assumptions shown in Figure 2.9. The data for the horizontal tendons generally confirms the assumed design force distribution. The surviving gages do not provide enough data points to fully define the shape of the force distribution curve, notably where the effect of the anchor set loss disappears. Due to the discontinuities in the hoop tendon force distribution, only the data points are shown and no attempt was made to interpolate the hoop tendon force between measurement locations. In general, the data is consistent with the design assumptions and does not appear to contradict the predicted response.

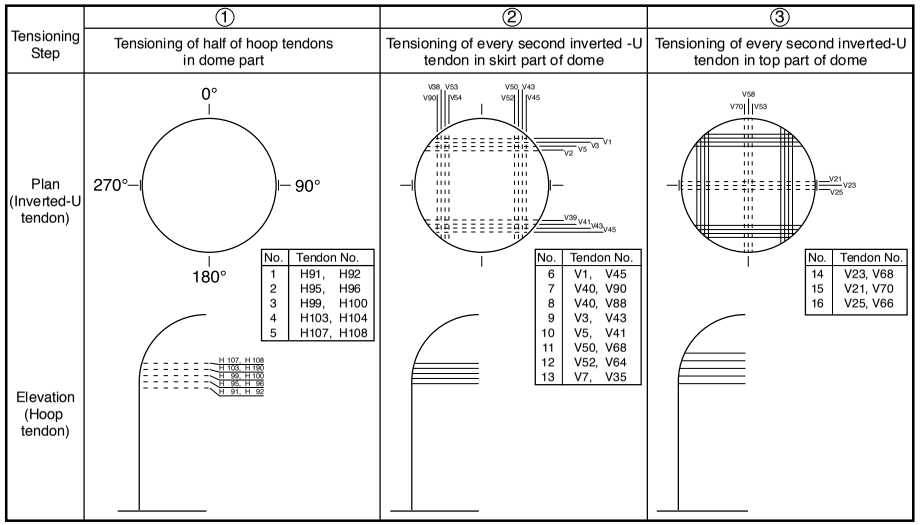

Tensioning Sequence (1/4)

Note: 1. Solid line shows tendon tensioned fully in the previous step.
2. Broken line shows tendon to be tensioned in this step.

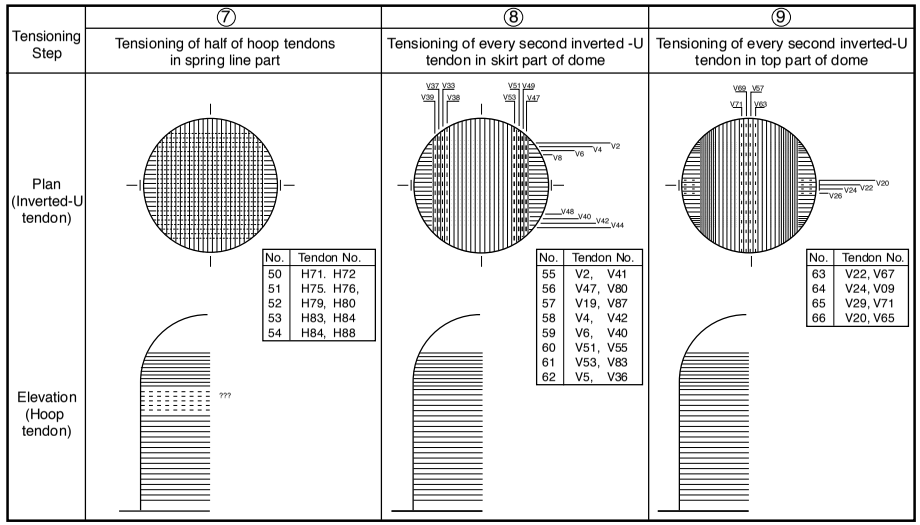

Tensioning Sequence (3/4)

Note: 1. Solid line shows tendon tensioned fully in the previous step.
2. Broken lines show tendon to be tensioned in this step.

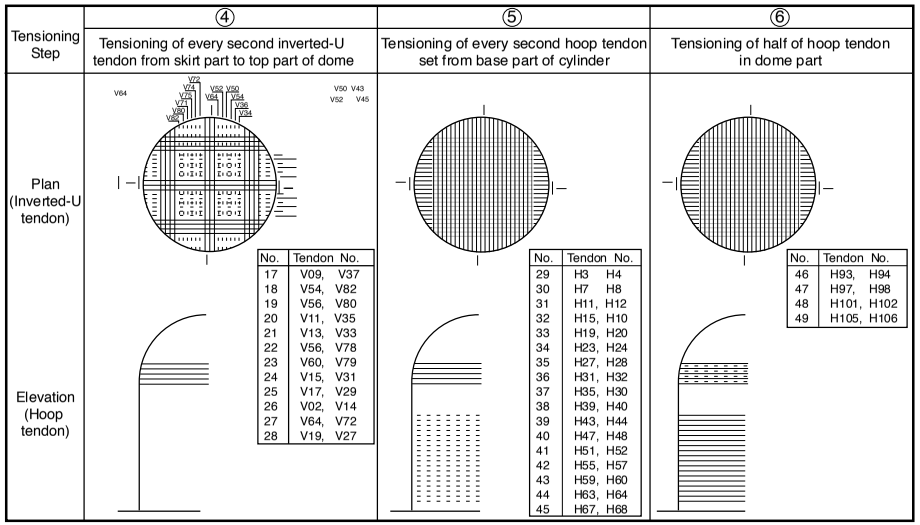

Tensioning Sequence (2/4)

Note: 1. Solid line shows tendon tensioned fully in the previous step.
2. Broken lines show tendon to be tensioned in this step.

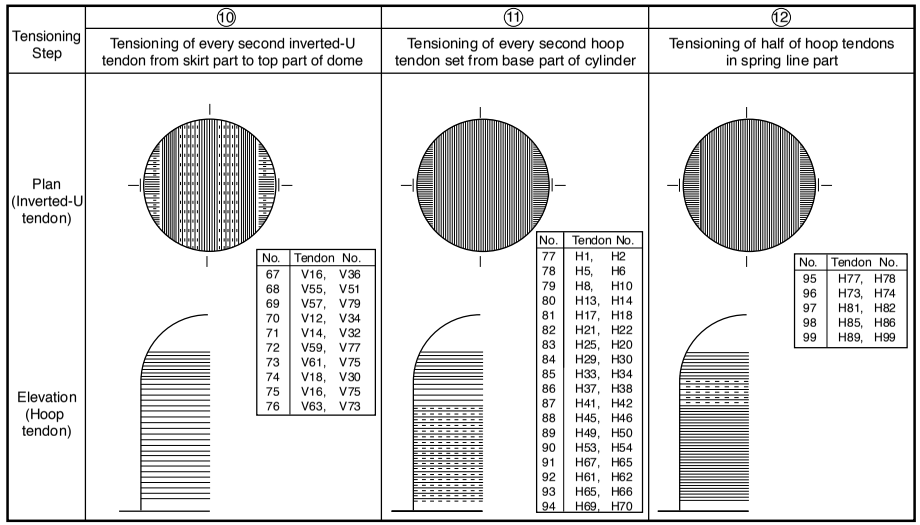

Tensioning Sequence (4/4)

Note: 1. Solid line shows tendon tensioned fully in the previous step.
2. Broken lines show tendon to be tensioned in this step.

Figure 2.56 PCCV Model Tensioning Sequence

Table 2.7 Model Prestressing Schedule

Sun	Mon	Tue	Wed	Thr	Fri	Sat
5-Mar	6-Mar	7-Mar	8-Mar	9-Mar	10-Mar	11-Mar
					H91 H92	
						V45
Sun	Mon	Tue	Wed	Thr	Fri	Sat
12-Mar	13-Mar	14-Mar	15-Mar	16-Mar	17-Mar	18-Mar
	H95 **H96** H99 H100 **H103**	**H103*** H104 H107* H108* **V1** *retensioning required	**V1*** V45* V90	**V46** V48 V88 V3 **V43**	V5 V41*(1)* V50	V86*(2)* V52 V84 **V7** V54
Sun	Mon	Tue	Wed	Thr	Fri	Sat
19-Mar	20-Mar	21-Mar	22-Mar	23-Mar	24-Mar	25-Mar
	V39 V23 V68 V21 V70 **V25***(3)* V66	V66* **V25 *(3)*** V9	**V37** ***NUPEC AUDIT INSP.*** V54 V82 V56* V80	V11 ***PRP SITE VISIT*** V35* **V13** V33 V58 V78 V60	V76* V15 **V31** V17 V29	V62 V74 V64 V72 **V19** V27 **H11**
Sun	Mon	Tue	Wed	Thr	Fri	Sat
26-Mar	27-Mar	28-Mar	29-Mar	30-Mar	31-Mar	1-Apr
	H3 **H4** H7* H8 H12	**H11** H16 *(4)* H15	H16 H19 H20 H23 H24 H27 H28 H31	H32 H36 **H35***(5)* **H40**	PS Op's suspended due to high winds.	**H63**
Sun	Mon	Tue	Wed	Thr	Fri	Sat
2-Apr	3-Apr	4-Apr	5-Apr	6-Apr	7-Apr	8-Apr
	H39* H44 H43 H48 H47 H52 H51	H56 H55 H60 H59 H64 H63*	**H63** **H67** **H68**	H93 H94 H97 H98 H102 H101	H105 H106	**V49**

Load Cell

Instrumented

Completed

Schedule Impact

**Tendon to be replaced

Weekend Milestone

Sequence

1	H91	58	**H4**
2	H92	59	H7**
3	H95	60	H8**
4	**H96**	61	**H11**
5	H99	62	H12
6	H100	63	H15
7	**H103**	64	H16
8	H104	65	H19
9	H107	66	H20
10	H108	67	H23
11	**V1**	68	H24
12	V45	69	H27
13	**V46**	70	H28
14	V90	71	H31
15	V48	72	H32
16	V88	73	**H35**
17	V3	74	H36
18	**V43**	75	H39
19	V5	76	**H40**
20	V41	77	H43
21	V50	78	H44
22	V86**	79	H47
23	V52	80	H48
24	V84	81	H51
25	**V7**	82	H52
26	V39	83	H55
27	V23	84	H56
28	V68	85	H59
29	V21	86	H60
30	V70	87	**H63**
31	**V25**	88	H64
32	V66	89	**H67**
33	V9	90	**H68**
34	**V37**	91	H93
35	V54	92	H94
36	V82	93	H97
37	V56	94	H98
38	V80	95	H101
39	V11	96	H102
40	V35	97	H105
41	**V13**	98	H106
42	V33	99	H71
43	V58	100	H72
44	V78	101	**H75**
45	V60	102	H76
46	V76	103	H79
47	V15	104	H80
48	**V31**	105	H83
49	V17	106	H84
50	V29	107	H87
51	V62	108	H88
52	V74	109	V2
53	V64	110	V44
54	V72	111	V47
55	**V19**	112	V89
56	V27	113	**V49**
57	H3		

Table 2.7 Model Prestressing Schedule (continued)

Sun	Mon	Tue	Wed	Thr	Fri	Sat
9-Apr	10-Apr	11-Apr	12-Apr	13-Apr	14-Apr	15-Apr
	Jack Re-calibration	PS Op's suspended due to high winds.	H71 H72 **H75** H76 H79 H80 H83 H84	H87 H88 V2 V44 V47* V89 **V49**	V87 V4 V42 V6*(1)* V40*(2)* V51	V12
Sun	Mon	Tue	Wed	Thr	Fri	Sat
16-Apr	17-Apr	18-Apr	19-Apr	20-Apr	21-Apr	22-Apr
	V85 Op Error damaged 19/31 gages. Op's suspended	Op's suspended	**V85** V53 V83	V8* V38 V22 **V67*** V24 V69	V26* V71 V20 V65 V10 V36	V36(6) **V55** V81 V57 H22
Sun	Mon	Tue	Wed	Thr	Fri	Sat
23-Apr	24-Apr	25-Apr	26-Apr	27-Apr	28-Apr	29-Apr
	V79* V12 V34 V14 V32*(6)* V59	V77 **V61*** V75 V16 V30 V18 V28 V63 **V73**	H1 H2 H5 H6 H9 H10 H13 H14	H17 H18 H21 H22 **H25** H26 H29 **H30** H33 H34 H37 H38	H41 H42 H45 **H46** H49 H50	H73
Sun	Mon	Tue	Wed	Thr	Fri	Sat
30-Apr	1-May	2-May	3-May	4-May	5-May	6-May
	H54 **H53** H57	**H58** H61 H62 H65 H66 H69 H70 H73 H74 H77 H78 H81 **H82**	H85 H86 **H89** H90 H90			

Sequence

114	V87	157	H9**
115	V4	158	H10
116	V42	159	H13
117	V6*(1)*	160	H14
118	V40*(2)*	161	H17
119	V51	162	**H18**
120	**V85**	163	H21
121	V53	164	H22
122	V83	165	**H25**
123	V8	166	H26
124	V38	167	H29
125	V22	168	**H30**
126	**V67**	169	H33
127	V24	170	H34
128	V69	171	H37
129	V26	172	H38
130	V71	173	H41
131	V20	174	H42
132	V65	175	H45
133	V10	176	**H46**
134	V36	177	H49
135	**V55**	178	H50
136	V81	179	**H53**
137	V57	180	H54
138	**V79**	181	H57
139	V12	182	**H58**
140	V34	183	H61
141	V14	184	H62
142	V32	185	H65
143	V59	186	H66
144	V77	187	H69
145	**V61**	188	H70
146	V75	189	H73
147	V16	190	H74
148	V30	191	H77
149	V18	192	H78
150	V28	193	H81
151	V63	194	**H82**
152	**V73**	195	H85
153	H1	196	H86
154	H2	197	**H89**
155	H5	198	H90
156	H6		

Notes:

(1) V41 removed and replaced with V6. V41 set-loss, friction and loft-off were high.
(2) V86 (mock-up tendon) removed and replaced with V40 tendon.

(3) Remove V25, friciton loss too high (>0.25), detension, remove LC's, remove and replace strand, reinstall LC's tomorrow (3/21) AM.
(4) Remove and replace tendon due to lift-off force too high.
(5) Tensioning of H35 delayed due to water in LC connectors, connectors removed and hardwired
(6) V36 removed and replaced, friction not within specifications.

Figure 2.57 Tensioning Hoop Tendons

Figure 2.58 Tensioning Hardware Assembly and Load Cell

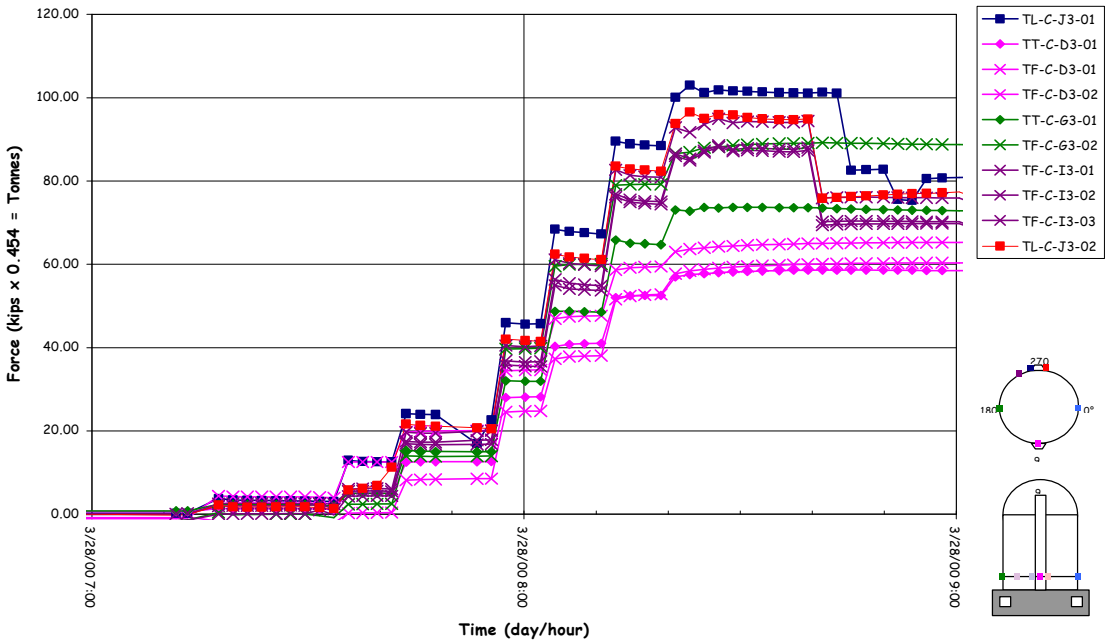

Figure 2.59 Tendon H11 Tensioning Force Time History

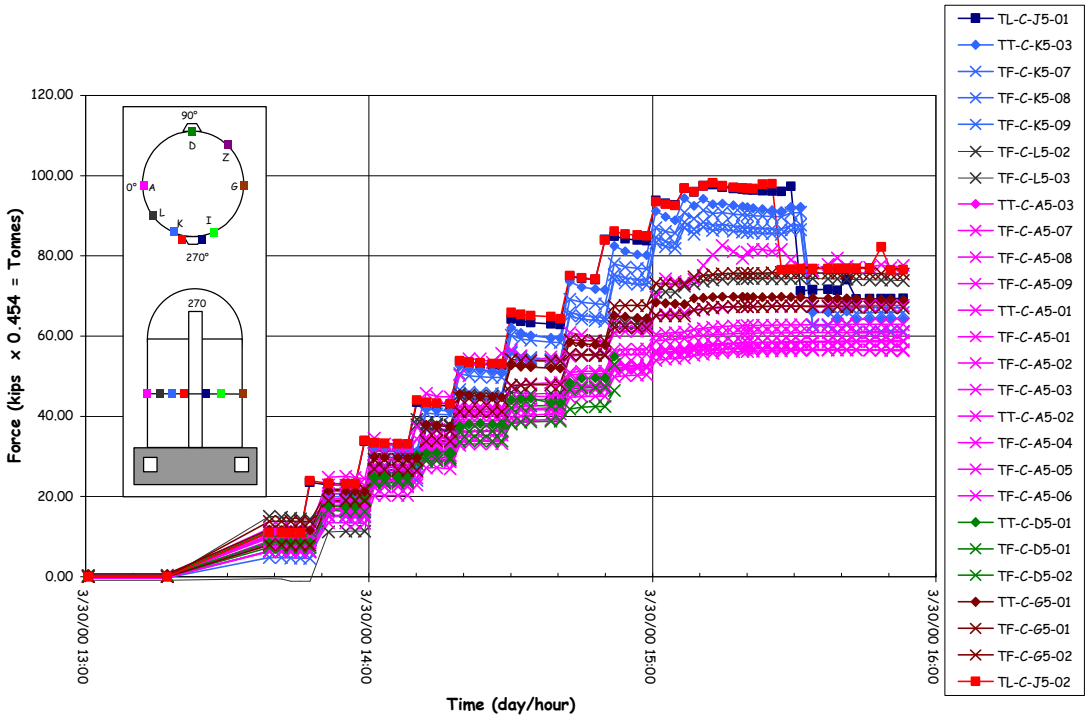

Figure 2.60 Tendon H35 Tensioning Force Time History

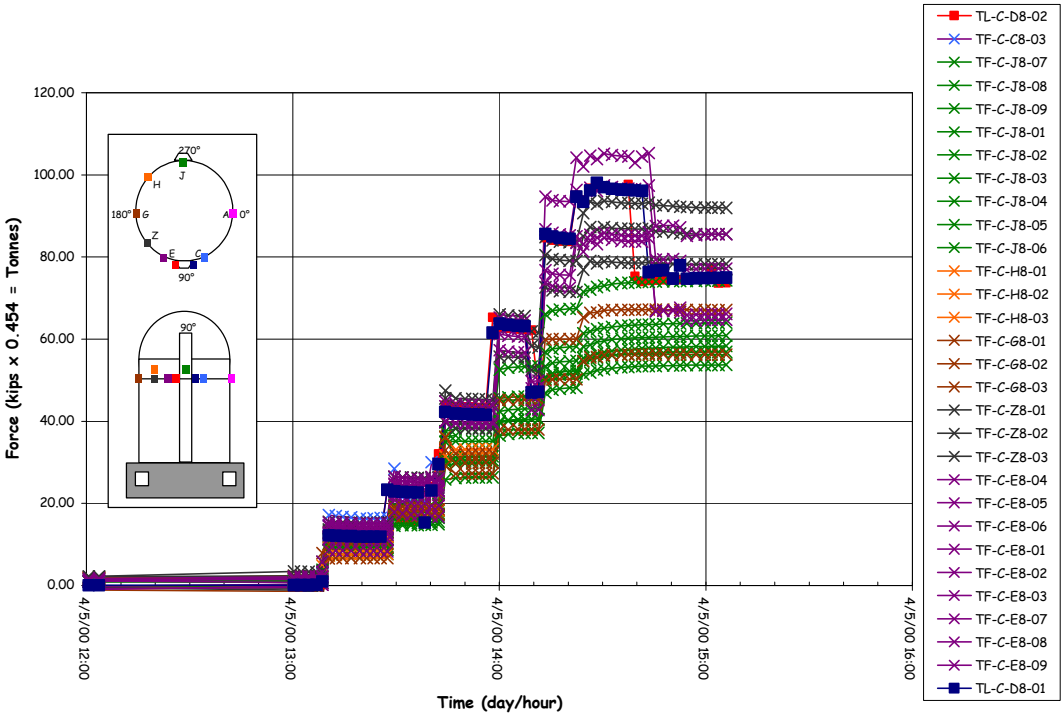

Figure 2.61 Tendon H53 Tensioning Force Time History

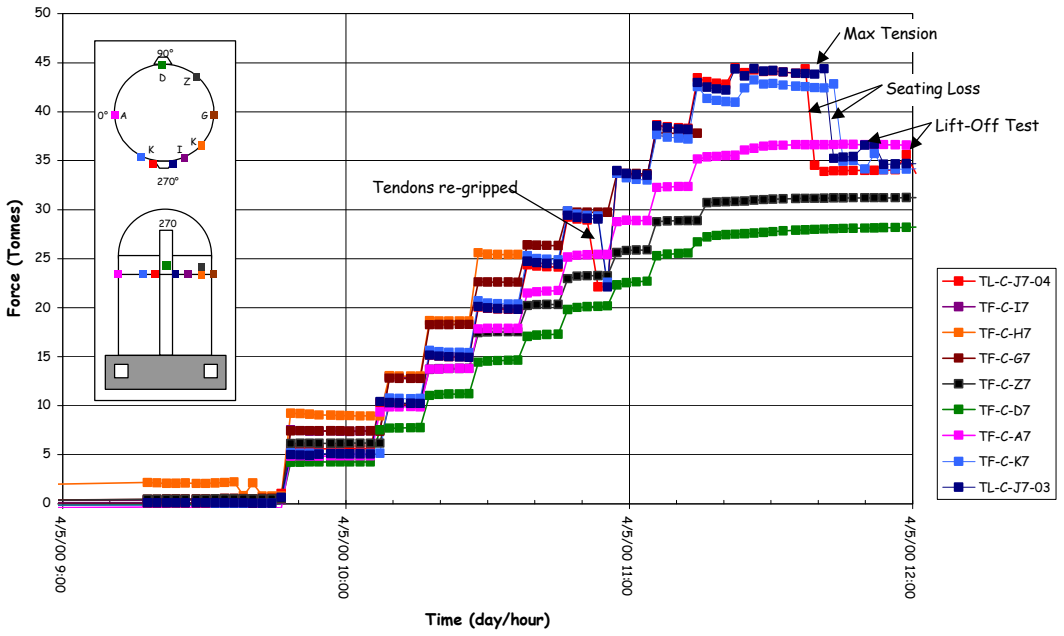

Figure 2.62 Tendon H67 Tensioning Force Time History

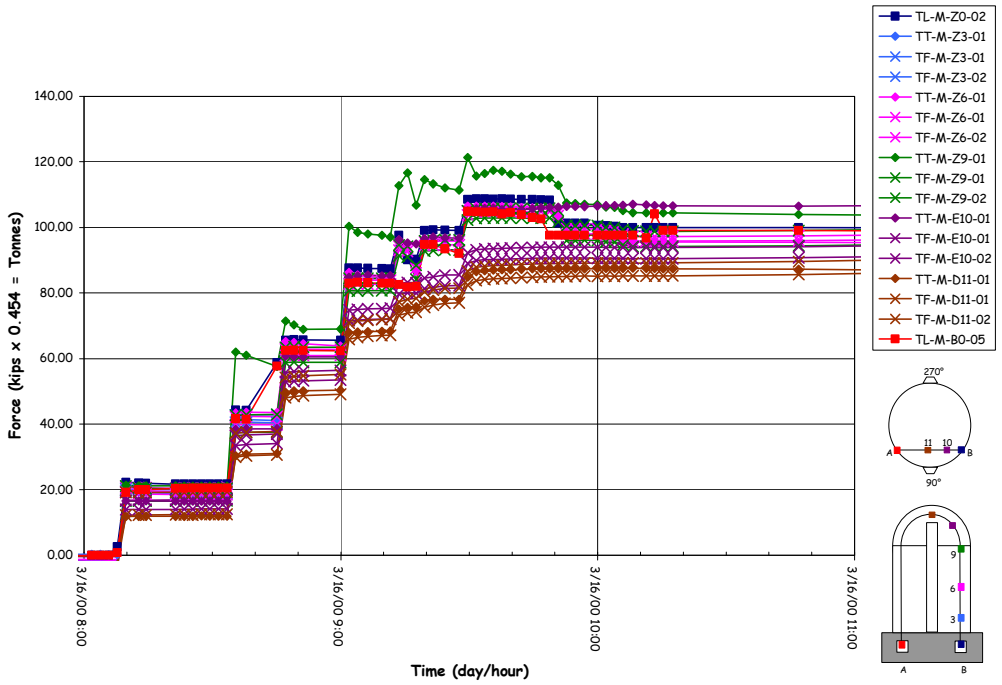

Figure 2.63 Tendon H68 Tensioning Force Time History

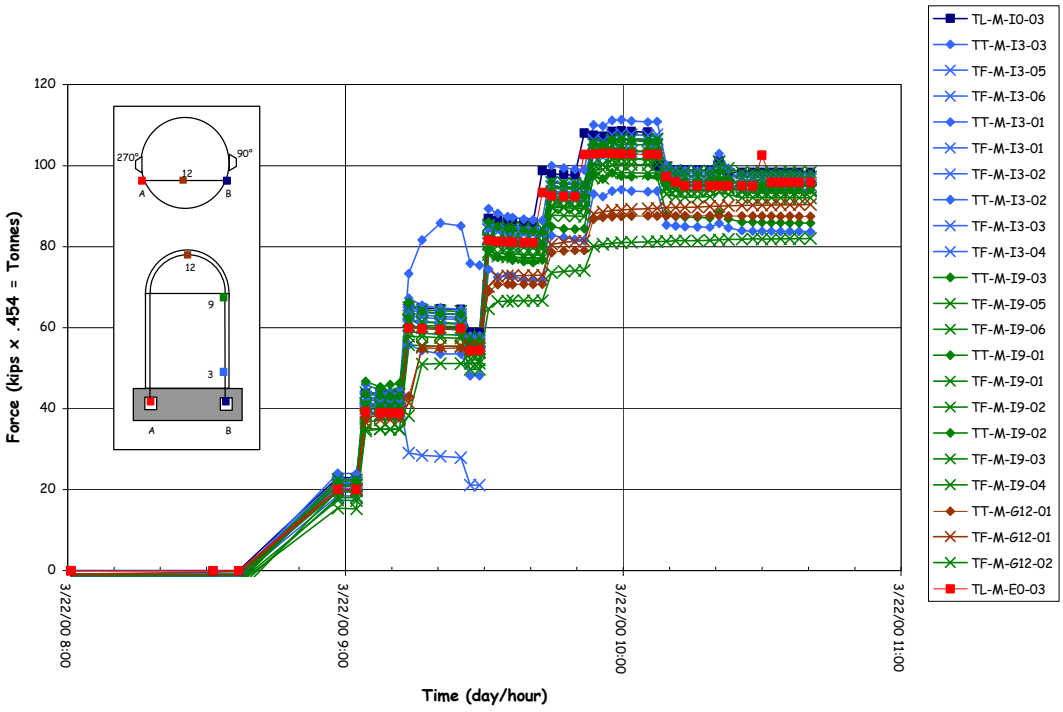

Figure 2.64 Tendon V37 Tensioning Force Time History

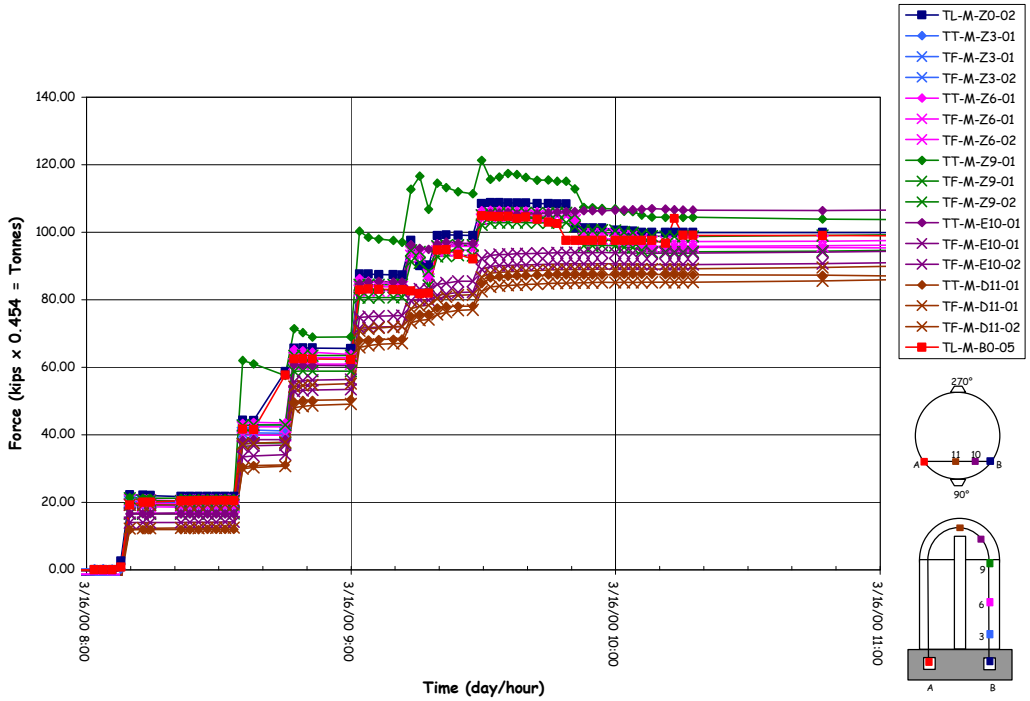

Figure 2.65 Tendon V46 Tensioning Force Time History

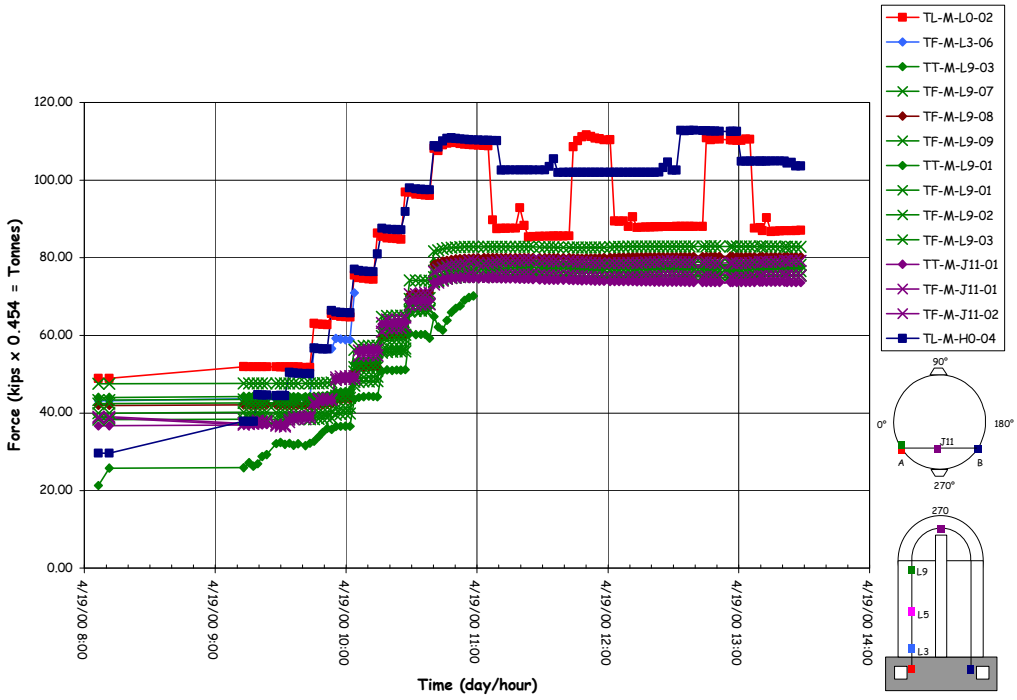

Figure 2.66 Tendon V85 Tensioning Force Time History

Table 2.8 Instrumented Tendon Gage Performance during Prestressing

H11:	4/12 strain gages failed	33% mortality
H35:	23/39 strain gages failed	59% mortality
H53:	14/22 strain gages failed	59% mortality
H67:	11/21 strain gages failed	52% mortality
H68:	18/33 strain gages failed	54% mortality
V46:	3/15 strain gages failed	20 % mortality
V85:	20/30 strain gages failed	67% mortality (operator error)
Overall*:	96/193 strain gages failed	50% mortality
*Six additional gages failed prior to pressure testing: (102/193, 53%)		

The vertical tendon data, however, appears to suggest that the wobble friction in the straight portion of the cylinder wall may be underestimated, while the angular friction in the dome may be overestimated. Since the majority of the strain gages on V37 and V46 survived and the force distribution is more nearly a continuous function, a curve was fitted through the test data to facilitate interpreting and comparing the design assumptions. Unfortunately, due to operator error prior to the start of prestressing operations, most of the gages on V85 (which is deflected around the E/H), were damaged. While the force distribution around the penetration was not obtained, it is apparent that deflecting the tendon around the penetration results in additional losses, as expected.

Finally, the prestressing contractor's data and the load cell data was summarized for comparison with the design specification in Table 2.9.

Table 2.9 Prestressing Data Summary

	Hoop Tendons		**Vertical Tendons**	
Average Tension Force:				
Design:	44.41 T	97.9 kips	49.57 T	109.3 kips
Jack:	43.53 T	95.97 kips	49.02 T	108.07 kips
Jack (w/ Load Cells only):	43.61 T	96.14 kips	49.09 T	108.23 kips
Load Cells:	43.21 T	95.27 kips	48.20 T	106.27 kips
Average Lift-off Force:				
Design:	34.11 T	75.2 kips	46.31 T	102.1 kips
Jacks:	34.02 T	75.01 kips	44.22 T	97.49 kips
Average Friction Coefficient:	0.18		0.22	
Average Seating Loss:	3.95 mm	0.16"	4.9 mm	0.19"
Jack:	9.51 T	20.96 kips	4.80 T	10.58 kips
Load Cell:	9.86 T	21.75 kips	4.64 T	10.23 kips
Average Final Load Cell Force:	33.34 T	73.52 kips	43.56 T	96.04 kips
Average Elastic Loss:	0.27 T	0.59 kips	0.58 T	1.29 kips

One Tonne = 1000 kg_f = 9.807 kN = 2.205 kips

Figure 2.67 H11 Tendon Force Distribution, Elev. 1854

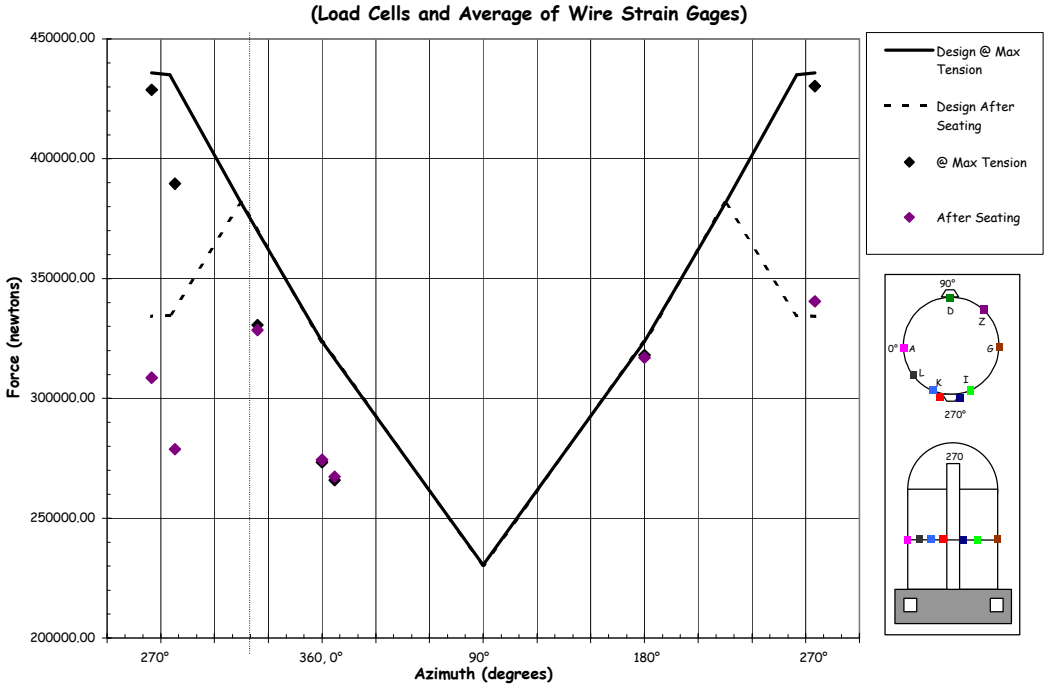

Figure 2.68 H35 Tendon Force Distribution, Elev. 4572

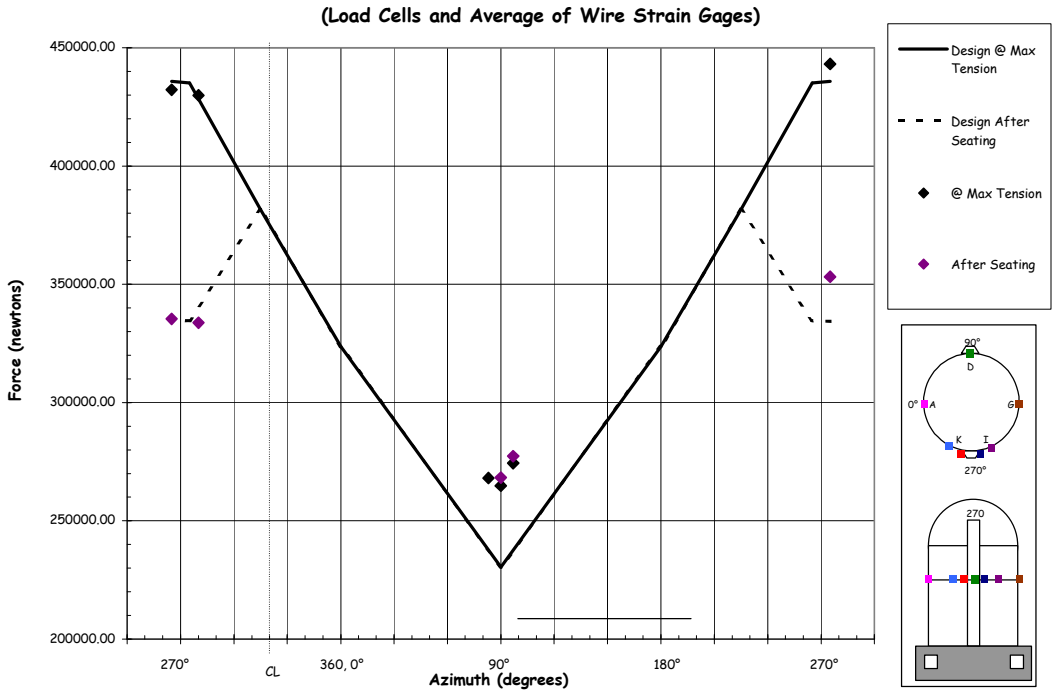

Figure 2.69 H53 Tendon Force Distribution, Elev. 6579

Figure 2.70 H67 Tendon Force Distribution, Elev. 8153

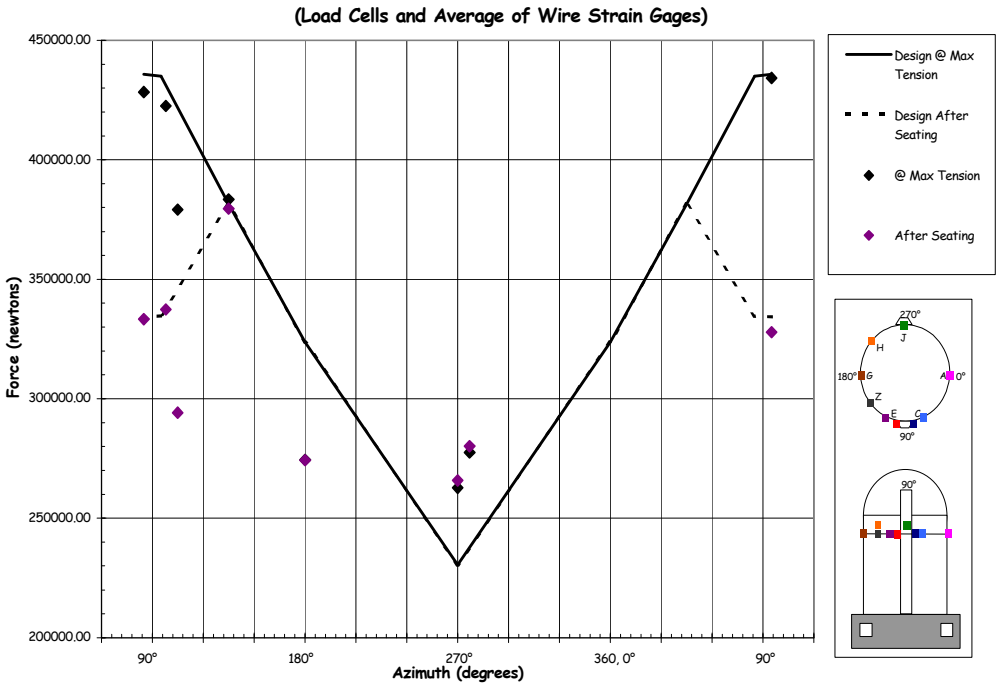

Figure 2.71 H68 Tendon Force Distribution, Elev. 8280

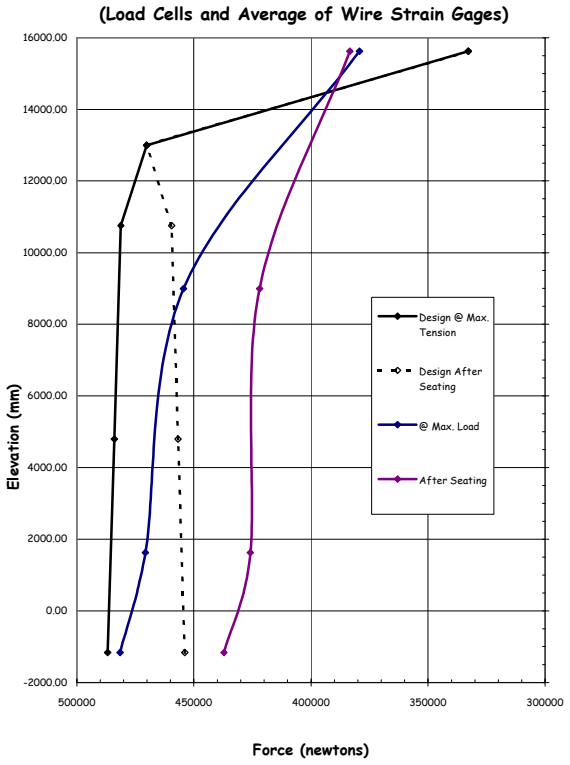

Figure 2.72 V37 Tendon Force Distribution, Azimuth 240 Degrees

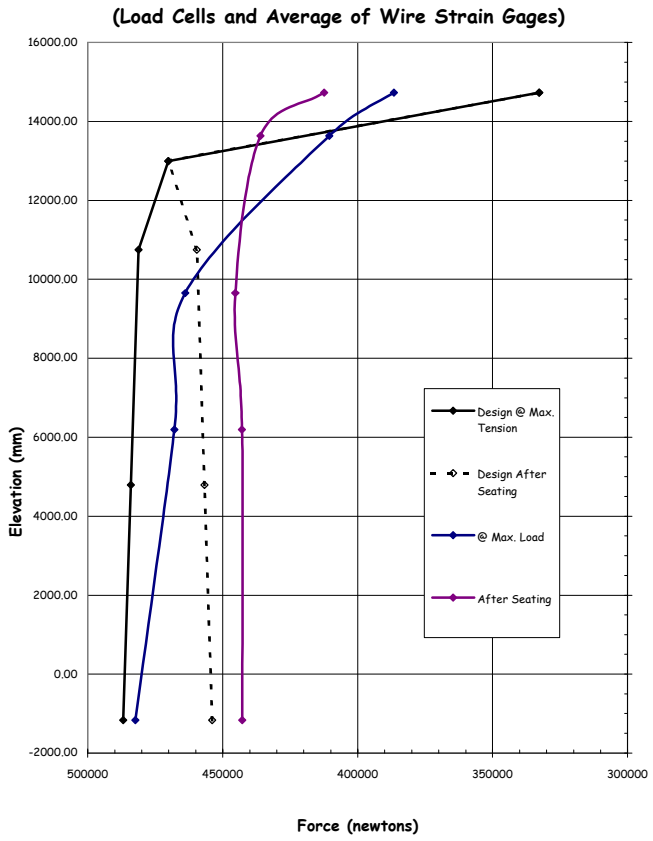

Figure 2.73 V46 Tendon Force Distribution, Azimuth 135 Degrees

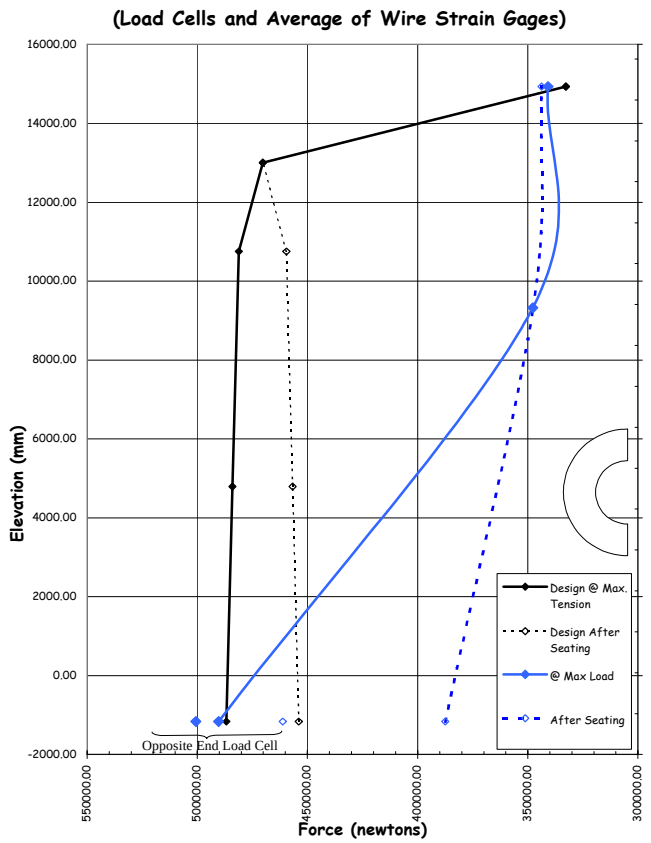

Figure 2.74 V85 Tendon Force Distribution, Azimuth 325 Degrees